Date 2012
Author Vermeiden, J.G., K. Kooiker, F.H. Lafeber,
T. van Terwisga, B. Cerup-Simonson and R. Folso
Address Delft University of Technology
Ship Hydromechanics and Structures Laboratory
Mekelweg 2, 2628 CD Delft

TUDelft

Delft University of Technology

A systematic experimental study on powering performance of flapping foil propulsors.

by

Vermeiden, J.G., K. Kooiker, F.H. Lafeber, T. van Terwisga, B. Cerup-Simonson and F. Folsø

Report No. 1891-P **2012**

Proceedings of the 29th Symposium on Naval Hydrodynamics, Gothenburg, Sweden, 26-31 August 2012.

29th SYMPOSIUM ON NAVAL HYDRODYNAMICS

AUGUST 26 - AUGUST 31
GOTHENBURG, SWEDEN

DETAILED PROGRAMME

29th Symposium on Naval Hydrodynamics - Preliminary Programme

Sunday, August 26	
17:00 - 21:00	Registration
19:00 - 21:00	Reception

Monday, August 27		
8:30 - 10:30	Introduction **Professor Karin Markides**, President, Chalmers University of Technology **Dr Clayton V. Stewart**, Technical Director, Office of Naval Research – Global Invited Lecture: Nature's Propulsion Methods **John Dabiri** Chair: Lars Larsson	
10:30 - 11:00	Coffee Break	
11:00 - 12:00	Parallel Sessions	
	Confined Water Hydrodynamics (2) Chair: Shin Hyung Rhee A Computational Study of Shallow-Water Effects on Ship Resistance **Hoyte Raven** Confined Water Effects on the Viscous Flow around a Tanker with Propeller and Rudder **Lu Zou, Lars Larsson**	**Fluid-Structure Interaction I (2)** Chair: Christer Fureby Optimal Design of Biologically -Inspired Foil Kinematics using Integrated CFD-CSD Simulations **Donghyun You, Jinmo Lee, Jiho You** Fully Coupled BEM-FEM Analysis For Ship Hydroelasticity in Waves **K.H. Kim, J.S. Bang, Y. Kim, S.J. Kim, Y.I. Kim**
12:00 - 13:00	Lunch	
13:00 - 15:00	Parallel Sessions	
	Propulsor Hydrodynamics I (4) Chair: Georges Chahine Quasi-Steady Two-Quadrant Open Water Tests for the Wageningen Propeller C- and D- Series **Jie Dang, Joris Brouwer, René Bosman, Christiaan Pouw** Bio-Inspired Propulsion: Efficiency Improvements in UUVs using a Starling Vortex Generator **Robert Whittlesey, John O. Dabiri** Numerical Simulation of	**Maneuvering and Control I (4)** Chair: Naoya Umeda Maneuvring Predictions in the Early Design Phase using CFD Generated PMM Data **Claus Simonsen, Janne F. Otzen, Christian Klimt, Nikolaj L. Larsen, Fred Stern** Comprehensive Prediction, Correlation, and Validation of Full-Scale Ship Performance in Waves **Craig Merrill, Christopher Bassler, Wil Faller, Kristine Beale**

	Wetted and Cavitating Flows inside Water-jets **Shu-Hao Chang, Spyros A. Kinnas** A Systematic Experimental Study on Powering Performance of Flapping Foil Propulsors **Jacques Vermeiden, K. Kooiker, F.H. Lafeber, T. Van Terwisga, B. Cerup-Simonsen, R. Folso**	System Based Simulation of Delft 372 Catamaran Maneuvering Characteristics as Function of Water Depth and Approach Speed **Evgeni Milanov, V. Chotukova, Frederick Stern** Investigation of Asymmetrical Shaft Power Increase during Ship Maneuvers by Means of Model Tests and CFD **Salvatore Mauro, G. Dubbioso, R. Broglia, R. Muscari**
15:00 - 15:30	Coffe Break	
15:30 - 17:30	Parallel Sessions	
	Viscous Ship Hydrodynamics I (4) Chair: Luis Eca A Velocity Decomposition Approach for Steady Free-Surface Flow **William Rosemurgy, D.O. Edmund, K.J. Maki, R.F. Beck** An Efficient Numerical Method for Estimation of Ship Roll Damping **Sven Handschel, Nikolai Köllisch, Jan Philip Soproni, Moustafa Abdel-Maksoud** Experimental and Computational Investigation of a Generic Conventional Submarine Hull Form **B. Anderson, M. Chapuis, L. Erm, C. Fureby, M. Giacobello, S. Henbest, D. Jones, M. Jones, C. Kumar, M. Liefvendahl, P. Manovski, D. Norrison, H. Quick, A. Snowden, A. Valyiff, R. Widjaja, B. Woodyatt** Analysis of Scale Effects in Ship Powering Performance using a Hybrid RANS-BEM Approach **A.R. Starke, J. Bosschers**	**Nonlinear Wave-induced Motions and Loads I (4)** Chair: Woei-Min Lin A Fluid Impulse Nonlinear Theory of Ship Motions And Sea Loads **Paul Sclavounos, Sungho Lee** Experimental Study on the Six Degree-of-Freedom Motion of a Damaged Ship for CFD Validation **Sungkyun Lee, Ji-Myoung You, Hyun-Ho Lee, Shin Hyung Rhee, Key-Pyo Rhee** Multi-Level Analysis on Parametric Roll in Regular and Irregular Waves **Yonghwan Kim, D.M. Park, K.H. Song, T.Y. Kim** Validation of Simulation-Based Approach for Predicting Ship Stability Failure Probabilities **William Belknap, B. Campbell, V. Belenky, T. Smith**

Tuesday, August 28		
8:30 - 9:30	Invited Lecture: Hydrodynamic mechanisms controlling cavitation erosion **Göran Bark** Chair: Ki-Han Kim	
9:30 - 10:00	Coffee Break	
10:00 - 12:00	Parallel Sessions	
	Propulsor Hydrodynamics II (4) Chair: Martin Hoekstra Study of End-Plate Shape Variations for Tip Loaded Propellers using a RANSE Solver **Antonio Sánchez-Caja, Juan González-Adalid, Mariano Pérez-Sobrino, I. Saisto** Prediction of Propeller Performance under High Loading Conditions with Viscous/Inviscid Interaction and New Wake Alignment Model **Spyros Kinnas, Xiangming**	**Fluid-Structure Interaction II (4)** Chair: Robert Beck Unsteady Fluid Structure Interaction Response of Marine Propellers in Crashback **Ronald Miller, Sung-Eun Kim, Bong Rhee, Julie Young** Fluid-Structure Interaction Response and Stability of Flexible Hydrofoils **Yin Lu Young, Eun Jung Chae, Antoine Ducoin, Ronald Miller, Sung Eun Kim**

	Yu, Ye Tian Performance and Vortex Formation of Flettner Rotors at High Reynolds numbers **Da-Qing Li, Michael Leer-Andersen, Björn Allenström** Simulation Based Analysis of the Hydrodynamics and Load Fluctuations of a Submarine Propeller behind a Fully Appended Submarine Hull **Mattias Liefvendahl, C. Troeng**	The Impact of a Plunging Breaker on a Partially Submerged Cube **Christine Ikeda, Thomas T. O'Shea, Kyle A. Brucker, David A. Drazen, Douglas G. Dommermuth, Thomas Fu, Anne M. Fullerton, James H. Duncan** A Coupled Approach for the Prediction of the Fluid-Structure Interaction Response of Simplified Surface Effect Ship Seals **Matthew Kramer, Y.L. Young**
12:00 - 13:00	Lunch	
13:00 - 14:00	Invited Lecture: Verification and Validation in Naval Applications **Luís Eça & Martin Hoekstra** Chair: Pablo Carrica	
14:00 - 14:15	Short Break	
14:15 - 15:45	Parallel Sessions	
	Cavitation and Bubbly Flows I (3) Chair: Chang-Sup Lee Eulerian Polydispersed Modeling of Bubbly Flows around Ships with Application to Athena R/V **Alejandro Castro, P.M. Carrica** CFD Validation for Super-Cavitating Flow around Two-Dimensional Cavitators **Sunho Park, Shin Hyung Rhee** Quantitative Measurements of Water Quality and Cavitation Phenomena in Cavitation Tunnels **Willfried Kröger, Stefan Borchert, Stephan Höhne, Nils Damaschke**	**Maneuvering and Control II (3)** Chair: Claus Simonsen Surface Ship Maneuvering Forces in Calm Water and Waves **David Greeley, Simmy Willemann** Complimentary EFD and CFD on Effects of Headwinds on Towing Tank Resistance and PMM Tests for ONR Tumblehome **S.M. Mousaviraad, S.S. Cook, P.M. Carrica, Y. Toda, F. Stern** CFD Maneuvering Prediction of a Twin Screw Vessel with Different Stern Appendages Configuration **Giulio Dubbioso, D. Durante, R. Broglia, A. Di Mascio**
15:45 - 16:15	Coffe Break	
16:15 - 17:15	Parallel Sessions	
	Cavitation and Bubbly Flows II (2) Chair: Krishnan Mahesh Prediction of Scale Effects in a Cavitating Propeller Flow **Sergey Yakubov, Bahaddin Cankurt, Patrick Schiller, Moustafa Abdel-Maksoud, Thomas Rung** Time Resolved X-Ray Densitometry for Cavitating and Ventilated Partial Cavities **Simo Mäkiharju, Marc Perlin, Steven L. Ceccio**	**Undersea Vehicle Hydrodynamics (2)** Chair: Thomas Fu Overset Simulation of a Submarine and Propeller in Towed, Self-Propelled and Maneuvering Conditions **Nathan Chase, Thad Michael, Pablo Carrica** Anatomy of Turbulent Flow around DARPA SUBOFF Body in a Turning Maneuver using High-Fidelity RANS Computations **Sung-Eun Kim, Bong Rhee, Ronald W. Miller**
18:00	Reception hosted by the Gothenburg Municipal Council	

Wednesday, August 29	
11:00 - 12:00	Sightseeing Boat Tour in Gothenburg
14:30 ~late	Boat Tour to Marstrand and Banquet at Marstrand Fortress

Thursday, August 30		
8:30 - 9:30	Weinblum Lecture: Hydrodynamic Study on Added Resistance using Unsteady Wave Analysis **Masashi Kashiwagi** Chair: Arthur Reed	
9:30 - 10:00	Coffee Break	
10:00 - 12:00	Parallel Sessions	
	Fundamentals of Fluid Dynamics in the Naval Context I (3) Chair: Masashi Kashiwagi An Experimental and Numerical Study on the Break -up of a Turbulent Liquid Wall Sheet **Erin Hackett, J.B. Carneal, D.W. Pfitsch, A.M. Fullerton, D.C. Walker, T.C. Fu, D.C. Wyatt, T.T. O'Shea, K.A. Brucker, D.G. Dommermuth** A Detailed Investigation of the Use of Neural Networks to Simulate Ocean Wave Propagation **Wil Faller, L. Rhymes, D.G. Dommermuth, D.C. Wyatt, T.C. Fu** Towards LES of High Reynolds Number External Flows on Unstructured Grids **Aman Verma, Krishnan Mahesh**	**Near- and Far-Field Ship Wave and Wake Hydrodynamics I (4)** Chair: Frederick Stern Validation of CFD Simulations for Unsteady Violent Free Surface Flows: Case of the Hydrodynamics around Rowing Blades **Alban Leroyer, Sophie Barre, Jeroen Wacker, Patrick Queutey, M. Visonneau, Jean-Michel Kobus** Development, Application and Validation of Hybrid URANS-LES Methods for Flow Simulation in the Ship Stern Area **Nikolai Kornev, A. Taranov, E. Shchukin, J. Springer, M. Palm, Yu. Batrak** Towards an Air Entrainment Model **Pablo Carrica, A.M. Castro, J. Li, M. Politano, M. Hyman** Air Entrainment and Multiphase Turbulence in the Bubbly Wake of a Transom Stern **Kelli Hendrickson, G. Weymouth, S. Banerjee, Dick Yue**
12:00 - 13:00	Lunch	
13:00 - 15:00	Parallel Sessions	
	Propulsor Hydrodynamics III (4) Chair: Moustafa Abdel-Maksoud Large Eddy Simulation of Crashback in Ducted Propulsors with Stator Blades **Hyunchul Jang, Krishnan Mahesh** Cavitation Phenomena within the Rotor Blade Passage of an Axial Waterjet Pump **David Tan, R.L. Miorini, J. Katz, J. Keller** Performance Prediction of a Nozzle Propeller **Liming Xia, Johan Lundberg, Rickard E. Bensow** Localization of Singing Noise Sources of the Marine Propeller using TDOA (Time Difference of Arrival) Method **Jaehyung Lee, Wook Rhee, Byoung-Kwon Ahn, Jong-Soo Choi, Chang-Sup Lee**	**Extreme Waves (4)** Chair: René Huijsmans Statistical Analysis of Simulated Ocean Waves with Varied Non-linearity **Christopher Kent, John O'Dea, Christopher Bassler, Lisa Minnick** A Wireless Sensor Network for Measuring Ship Responses in Abnormal Waves **Sally Bennett, B. Winden, C.J. Brooks, S.R. Turnock, D.A. Hudson, A.I.J. Forrester, D.J. Taunton** Analysis of Wave Breaking Events Generated as a Result of a Modulational Instability **Alessandro Iafrati, Miguel Onorato, Alexander Babanin** Autoregressive Modeling of Ocean Waves **Alexander Degtyarev, Arthur Reed**
15:00 - 15:30	Coffe Break	
15:30 - 17:00	Parallel Sessions	
	Hydrodynamic Optimization in Ship Design I (3) Chair: Susanne Abrahamsson CFD-Based Multiobjective Stochastic Optimization of a Waterjet Propelled High	**Hydrodynamics of Fast or Unconventional Ships (3)** Chair: Lawrence Doctors Surface-Effect-Ship Bow-Seal High-Reynolds Number Experiments

	Speed Ship **Yusuke Tahara, Hiroshi Kobayashi, Manivannan Kandasamy, Wei He, Daniele Peri, Matteo Diez, Emilio Campana, Frederick Stern** Simulation Based Design with Variable Physics Modeling and Experimental Verification of a Waterjet Propelled Catamaran **Daniele Peri, M. Kandasamy, Y. Tahara, W. Wilson, M. Miozzi, E.F. Campana, F. Stern** Trajectories and Local Flow Field Measurements around ONR Tumblehome in Maneuvering Motion **Yugo Sanada, Yasuyuki Toda, Lichuan Gui, Kenji Tanimoto, Frederick Stern**	**Andrew Wiggins, Steven F. Zalek, Lawrence J. Doctors, Marc Perlin, Steven L. Ceccio, Robert J. Etter, Robert A. Wilson** A Detailed Assessment of Numerical Flow Analysis (NFA) to Predict the Hydrodynamics of a Deep-V Planing Hull **Thomas Fu, T.T. O'Shea, C.Q. Judge, D.G. Dommermuth, K. Brucker, D. C. Wyatt** EFD Measurements of the Velocity Field around the DELFT 372 Catamaran in Steady Drift **Riccardo Broglia, G. Aloisio, M. Falchi, S. Grizzi, S. Zaghi, M. Felli, M. Miozzi, F. Pereira, F. Di Felice**
18:00	Reception hosted by Berg Propulsion	

Friday, August 31		
8:30 - 9:30	Invited Lecture: Computational Ship Hydrodynamics: Status, Opportunities, and Challenges **Fred Stern** Chair: Patrick Purtell	
9:30 - 10:00	Coffee Break	
10:00 - 11:30	Parallel Sessions	
	Cavitation and Bubbly Flows III (3) Chair: Klas Brännström Investigation of Partial Cavitation and Its Transition to Cloud Cavitation using Time Resolved X-Ray Densitometry **Harish Ganesh, Simo Mäkiharju, Bu-Geun Paik, Steven L Ceccio** A Compressible Model for Cavitating Flow: Comparison between Euler, RANS and LES Simulations **Claes Eskilsson, Rickard E. Bensow** Vortex Cavitation Inception Delay by Local Polymer Injection **Georges Chahine, C-T Hsiao, X. Wu, Q. Zhang, J. Ma**	**Nonlinear Wave-induced Motions and Loads II (3)** Chair: Ricardo Broglia Effect of Hull Forms above Calm Water Plane on Extreme Ship Motions in Stern Quartering Waves **Tomohiro Furukawa, Naoya Umeda, Akihiko Matsuda, Daisuke Terada, Hirotada Hashimoto, Frederick Stern, Motoki Araki, Hamid Sadat Hosseini** Development and Validation of Numerical Simulations of Motions and Loads for Ships in Damaged Conditions **Kenneth Weems, Allen Engle, Woei-Min Lin** Split Time Method for the Probabilistic Characterization of Stability Failures in Quartering Seas **Vadim Belenky, Kostas Spyrou, Kenneth M. Weems, Woei-Min Lin**
11:30 - 12:30	Lunch	
12:30 - 13:30	Parallel Sessions	
	Viscous Ship Hydrodynamics II (2) Chair: Hoyte Raven High-Fidelity Curvilinear-Grid Two-Phase Flow Solvers for Ship Hydrodynamics **Jianming Yang, Zhaoyuan Wang, Seongmo Yeon, Bonguk Koo, Frederick Stern** Sliding Grids and Adaptive Grid Refinement Applied to Ship Hydrodynamics **J. Wackers, G.B. Deng, P.**	**Near- and Far-Field Ship Wave and Wake Hydrodynamics II (2)** Chair: Yusuke Tahara Numerical and Experimental Study of Bubble Entrainment due to a Horizontal Plunging Jet **Chao-Tsung Hsiao, X. Wu, J. Ma, G.L. Chahine** Formation of Corner Waves in the Wake of a Partially Submerged Bluff Body **Pablo Martinez-Legazpi, Javier Rodriguez-**

	Queutey, M. Visonneau, E. Guilmineau	**Rodriguez, A. Korobkin, Juan Lasheras**
13:30 - 13:45	Short Break	
13:45 - 14:45	Parallel Sessions	
	Propulsor Hydrodynamics IV (2) Chair: Rickard Bensow Waterjet Thrust Augmentation using High Void Fraction Air Injection **Xiongjun Wu, Sowmitra Singh, Jin-Keun Choi, Georges L. Chahine** Hydrodynamics of Twin Screw Vessels with Feathered Propellers **Tobias Huuva, Olof Klerebrant Klasson, Magnus Pettersson**	**Fundamentals of Fluid Dynamics in the Naval Context II (2)** Chair: Emilio Campana An Extended Wind Boundary Layer Profile **A.M. Fullerton, K.L.C. Beale, E.J. Terrill, D.G. Dommermuth** Numerical Simulation of Internal Tide Generation at a Continental Shelf Break **Laura Brandt, James W. Rottman, Kyle A. Brucker, Douglas G. Dommermuth**
14:45 - 15:15	Coffee Break	
15:15 - 16:15	Parallel Sessions	
	Hydrodynamic Optimization in Ship Design II (2) Chair: Peter Grundevik Hydrodynamic Optimization of Pre-swirl Stator by CFD and Model Testing **Keunjae Kim, Michael Leer-Andersen, Sofia Werner, Michal Orych, Youngbok Choi** Uncertainty Quantification of Delft Catamaran Added Resistance and Motions for Variable Regular and Irregular Head Waves and Geometry **Wei He, Matteo Diez, Daniele Peri, Emilio F. Campana, Yusuke Tahara, Frederick Stern**	**Innovations in Drag Reduction (1)** Chair: Chao-Tsung Hsiao Hydrodynamics of a Displacement Air Cavity Ship **Abolfazl Shiri, Michael Leer-Andersen, Rickard E. Bensow, Jacob Norrby**

Hosted by
CHALMERS

29th Symposium on Naval Hydrodynamics
Gothenburg, Sweden, 26-31 August 2012

A Systematic Experimental Study on Powering Performance of Flapping Foil Propulsors

J. G. Vermeiden (Civis Orbis BV, Netherlands),
K. Kooiker, F.H. Lafeber, T. van Terwisga (MARIN, Netherlands),
B. Cerup-Simonsen, R. Folsø (A.P. Møller Maersk A/S, Denmark)

Abstract

A near-optimal flapping propulsor was designed for a container-feeder ship, in order to assess possible efficiency gains within practical constraints. Performance of this flapping propulsor was measured in open water conditions at scale 1/12th by varying systematically Loading, Pitching amplitude, Chord-length, Chord-wise flexibility and Fin-spacing. A large improvement was measured resulting in an efficiency of 81% for the flapping propulsor at proper loading compared to 63% for the design screw-propeller. The efficiency gain due to chord-wise flexibility was smaller than expected, and the sensitivity of efficiency to chord-length was much larger than expected. This results in an optimal configuration from the point of view of hydrodynamics that yields fins with short chords operating at high transverse acceleration. Detailed data is made available on the performance of flapping fins in the selected range of parameters.

1. Introduction

The paper summarizes the results of a comprehensive experimental study on open water performance of flapping foil propulsion aimed at seagoing ships. In the chosen propulsion method, one or more near-vertical fins propel the ship in a combined movement of transversal heave and rotation along the near-vertical fin-stock. A container feeder ship was selected as a demonstration case where a systematic attempt was made to achieve a large (20%) gain in measured propulsive efficiency compared to state of the art screw-propellers to justify needed future development cost. A near optimal flapping propulsor was designed to fit within the geometric constraints of its hull at a representative ship speed. This design was based on public domain knowledge. The resulting Flapping Foil system has subsequently been tested at model scale in open water conditions for a range of systematically varied parameters.

Observed propulsive efficiencies in modern efficient ships (in 2012 typically 55% for self-propelled barges, 67% for tankers & bulkers, 73% for container carriers) display a large gap with the practical theoretical limit, dictated by an ideal propulsor that does not protrude from the bottom or from the sides of the ship. That ideal actuator would have an actuator area sized *Draught_ship.Width_ship*, resulting in low thrust coefficients $0.05<C_T<0.1$ and an ensuing ideal efficiency of 98%.

A conventional propeller utilizes 5% to 15% of the potentially available actuator surface in a ship. A flapping propulsor can sweep a large area, resulting in:

- Low axial kinetic energy losses because thrust is obtained by accelerating a large amount of water
- Low viscous losses because of the possibility for smaller non dimensional blade-surface at lower flow speeds due to higher lift coefficients
- Low downwash-caused losses as outlined by Katz & Weihs (1978)

Experimental work done by Sherer (1968) showed that fins of modest aspect ratio ($AR = 3$) and with moderate heave amplitude (*heave / chord* = 0.6) attain a flapping efficiency of 55%. Modeling work done by Katz & Weihs (1978) initiated understanding of the role of chord-wise flexibility in flapping propulsion, and opened a perspective for high-efficiency flapping propulsors. Measurements done at MIT with the participation of Triantafyllou from 1991 to 2005 for flapping propulsion with a rigid fin with $AR = 6$ displayed efficiencies up to of 70%, and resulted in sensitivities concerning the effect of varying:

- Phase-angle between heave and rotation
- Ratio chord / heave
- The cycle of angle of attack.
- Chord-wise flexibility

These high efficiencies were observed at Reynolds = 4.10^5, where viscous losses are materially higher than at the conditions seen in an actual ship, where the fins would operate at Reynolds $\approx 10^7$.

In applying flapping propulsion to merchant ships, it was found that a number of aspects were not covered in previous studies, and would be elemental to

validate many efforts of CFD oriented research, and to allow industry to make well informed evaluations:

- The effect of high Reynolds number over the foils
- The effect of variations in chord length
- Optimized cycles of angles of attack
- The effect of multi-fin operation and fin spacing
- Further characterization of chord-wise flexibility.

2. Design

Working case: a container feeder

A container feeder with good propulsive efficiency was selected as a working case. The hull of the container feeder was redesigned to accommodate an actual design of near-optimal flapping propulsor. To enable both steering and propulsion through the fins, choice was made for a transversal heave-motion like a fish-tail rather than like a sea-mammal. This results for the hull in a barge-stern at unchanged hull length, unchanged width, unchanged volume, an unchanged LCB, and a maximum flat width of the hull at the propulsor location of 23.18 m.

The investigated configuration has a single translating chariot that can power between 1 and 6 synchronously rotating fins at an effective stroke of 4.753 m, and actuator width varying between 4.753 m and 11.898 m depending on choice of filled fin-slots, a fin-span of 5.616 m, and an immersion at design conditions of 2.25 m with the flat top of the fins being held close to the hull to benefit from hull-effect for downwash minimization. The maximum actuator width with the machine is limited to 11.9 m due to the choice of a sealing-plate to separate the engine room from the sea; a design with roll-up seal could increase width.

Although measurements have been done with the limitations caused by the need to accommodate the mechanical propulsor in the described ship, this paper focuses on results obtained with open water conditions.

The mechanism and the cycle of angle of attack

The combined constant forward speed of the ship and periodic sideways movement of the fins causes periodic variation in orientation of the fins with the forward direction. To propel, the flapping propulsor must generate lift on the fins, which in turn is generated by angle of attack: the flapping propulsor must make the fins rotate synchronously with the varying flow-angle, but less than the said flow-angle (figure 2); if the fins rotate more we create a turbine.

Table 1. Ship & propeller characteristics

Container-feeder data		**Propeller data**	
Width	27.8 m	Diameter	5.7 m
Draught	8.25 m	Hub diameter	1.12 m
Design speed	10.13 m/s	Number of blades	6
Needed thrust	928 kN	Total blade surface	17.6 m^2
Est. needed thrust with flapping propulsor	800 kN	J_{design} = V/DN	0.585
		Open water efficiency	63%
		Blade AR	1.8

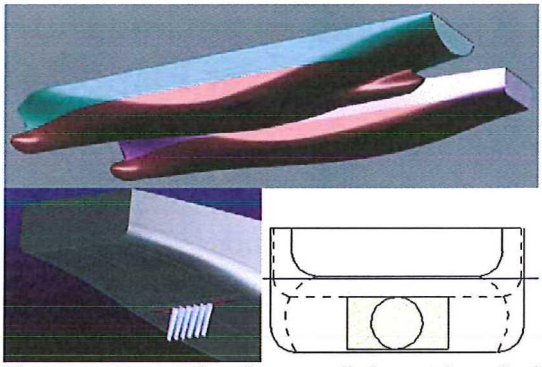

Figure 1: Conventionally propelled container feeder and modification for flapping propulsion

The periodic flow-angle at the fins is affected by the speed of the vessel and by frequency of heave. A good flapping propulsor will perform efficiently in a broad range of speed and loading. To achieve that, the machine needs to have a rotational movement approaching the rate of change of periodic flow-angle, but with lower amplitude to keep the angle of attack at a relatively constant value throughout each half-cycle. One objective for the program being ruggedness and mechanical simplicity, a solution was sought for single shaft drive for both the heave motion of the fins and their rotational cycle. The single-shaft mechanism in Figure 3 has a rotational movement of the same expression as the flow-angle; the rotation center of the

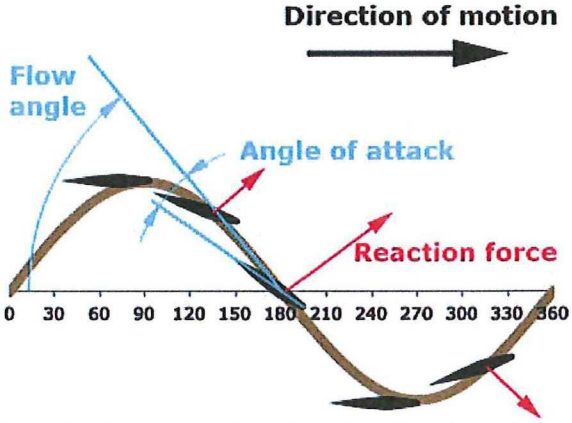

Figure 2: Flow angle and rotational position of the fins

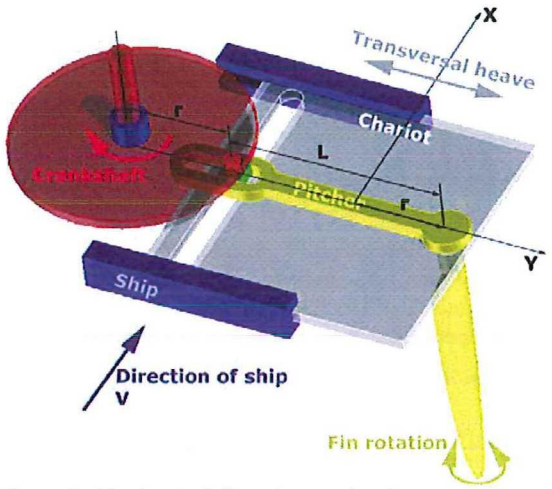

Figure 3: Single-shaft flapping mechanism

pitcher is on the bisector of the extreme positions of the crank on the chariot, and the sliding grove is perpendicular to the direction of heave.

With the conventions as drawn in Figure 3, the X component of the flow is V, and the Y component of the flow is $r.\omega.sin(\omega t)$ if the angular speed of the crankshaft is ω and t=0 is taken when the crank is at the drawn position, resulting in a defined flow angle as in expression (1). In the mechanism, the rotation angle of the fin with the direction of forward motion is equal to the angle of the pitcher with the Y axis. The Y component of the pitcher angle is constant in time at value L, and the X component of the pitcher angle varies in time with the value $r.sin(\omega t)$, resulting in a defined rotation angle of the fin as in expression (2). The angle of attack of the fin at the rotation axis of the fins is then the flow angle diminished by the rotation angle as in expression (3), as can be seen in figure 2.

$$\alpha_{flow} = Atan\left(\frac{r\omega}{V}\sin(\omega t)\right) \quad (1)$$

$$\alpha_{fin} = Atan\left(\frac{r}{L}\sin(\omega t)\right) \quad (2)$$

$$\alpha_{attack} = Atan\left(\frac{r\omega}{V}\sin(\omega t)\right) - Atan\left(\frac{r}{L}\sin(\omega t)\right) \quad (3)$$

The flow angle α_{flow} and the rotation angle of the fin α_{fin} have a close mathematical relationship: if $L = V/\omega$, $\alpha_{attack} = 0$ throughout the cycle. Figure 4 shows that the mechanism yields a cycle of angle of attack without the characteristic wobble documented by Hover, *et al.*, (2004) compared to a mechanism that would combine harmonic heave and harmonic rotation of the fins[1].

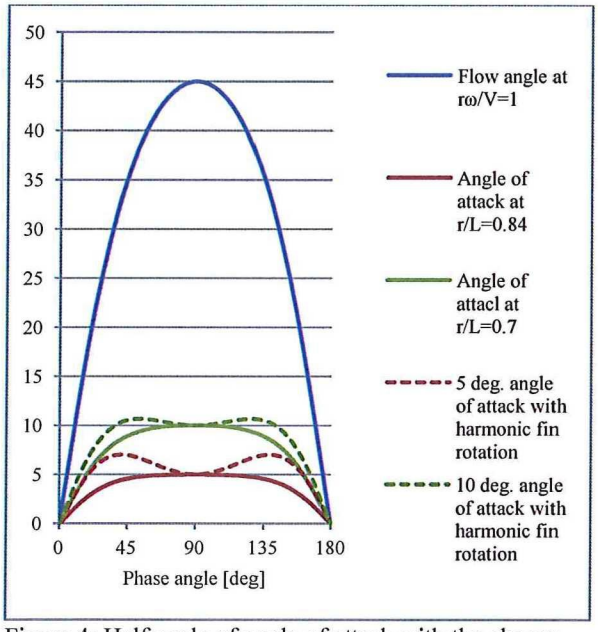

Figure 4: Half cycle of angle of attack with the chosen mechanism versus cycle with harmonic fin rotation

The outlined mechanism was embodied in a multi-fin configuration with continuously variable pitcher-length, continuously variable rotational offset for steering, flywheel with step-wise variably moment of inertia, transverse momentum impulse cancellation, and plate-seal to provide undisturbed flow along the hull. Variable parameters of the system are not meant to vary within the cycle.

Non-dimensional characterization

In ship powering, the ITTC provides guidelines for performance prediction based on measurements at scale[2]. The diameter D of the screw-propeller is used for characteristic length, and $D.N$ is used as characteristic speed, which results in the well known expressions for non-dimensional speed J, non-dimensional thrust K_T, and non dimensional input power K_Q, and the usual expression with non-dimensional terms:

$$\eta_{openwater} = \frac{Thrust * Speed}{Torque * Angular\_speed} = \frac{T.V_{advance}}{Q.\omega} = \frac{K_T.J}{2\pi K_Q} \quad (4)$$

[1] Harmonic heave is commonly utilized in measurement programs involving flapping propulsion

[2] ITTC, Performance, Propulsion, 1978 ITTC Performance Prediction method

The ITTC approach is built on the fact that due to fixed geometry of a metal screw-propeller, the values of K_T and K_Q only depend on J. This means that by keeping the frequency constant, and varying J, a complete dataset for the open-water performance of the propeller needs only a dozen measurements or so. In the case of flexible geometries such as flapping propulsors with chord-wise flexible fins, this approach is invalid: K_T and K_Q then vary separately with J and dynamic pressure, due to variation in lift coefficient caused by change in camber, in turn due to dynamic-pressure dependent bending.

We therefore need to define a dimensionless term E_2 that adequately represents bending behavior of the fins (see paragraph on fins). Having defined E_2 we modify the approach to include explicitly the velocity term $V_{advance}$. The propeller diameter is replaced by the total stroke $D=2r$ of the flapping motion. The advance ratio J, and the thrust coefficient C_T then become logical terms. Defining a dimensionless torque coefficient C_Q, we can investigate open water efficiency as a function of C_T, J, and E_2:

$$\eta_{openw.} = \frac{Thrust * Speed}{Torque * Angular\_speed} = \frac{T.V_{advance}}{Q.\omega}$$

$$= \frac{\frac{T}{\frac{1}{2}.\rho.S_{actuator}.V_{advance}^2} \cdot \frac{V_{advance}}{N.D}}{\frac{Q.2.\pi.N}{\frac{1}{2}.\rho.S_{actuator}.V_{advance}^2.N.D}} = \frac{C_T.J}{C_Q} \qquad (5)$$

In flapping propulsion, the actuator area depends on Fin-stroke (= crankshaft diameter in our machine), Fin-span, Number of fins installed and Fin-spacing. This is different from screw-propellers where the actuator area only depends on diameter, and is not dependent on the number of propeller blades. We therefore have no choice but to define 2 sets of coefficients: a thrust coefficient for a single fin $C_{T\text{-}fin}$ connected to C_{Q_fin} and a thrust coefficient for the complete propulsor C_T connected to C_Q.

C_T and J are convenient to utilize at this stage because they are well known in the performance prediction industry. Furthermore, the value of C_T gives an immediate link to the magnitude of impulse losses and gives an immediate link to the forward flow-speed V_{X_flow} through actuator disk theory:

$$\eta_{ideal} = \frac{2}{1+\sqrt{1+C_T}}; V_{X_{flow}} = \frac{V_{advance}}{\eta_{ideal}} \qquad (6)$$

At given advance ratio J, the non-dimensional thrust C_T is achieved through setting the proper rotational amplitude of the fins. We define the critical advance ratio of the machine as the advance ratio J_c where there is no angle of attack throughout the cycle, and substituting in (2). This definition of J_c fits the chosen machine because the cycle of angle of attack has the same expression as the cycle of flow-angle.

$$J_c = \frac{2.\pi.L_{pitcher}}{D}; \alpha_{fin} = Atan\left(\frac{\pi}{J_c}\sin(\omega t)\right) \qquad (7)$$

By substitution of (6) and (7) in (1) and (3), we also obtain estimators for the flow-angle and the angle of attack of the fins throughout the cycle in the case of open water measurement:

$$\alpha_{flow} \approx Atan\left(\frac{\pi.\eta_{ideal}}{J}\sin(\omega t)\right) \qquad (8)$$

$$\alpha_{attack} \approx Atan\left(\frac{\pi.\eta_{ideal}}{J}\sin(\omega t)\right) - Atan\left(\frac{\pi}{J_c}\sin(\omega t)\right) \qquad (9)$$

At given fin-span and crankshaft-diameter (= fin-stroke), we can now measure thrust coefficient and open water efficiency as a function of (J, J_c, E_2), which are all input parameters. We could equally well have chosen to characterize the path of the fins non-dimensionally by *Strouhal* = *1/J* as is often utilized in studies for flapping locomotion and propulsion. We chose to stick to existing custom in ship powering.

Fin characteristics including bending characteristic E_2

Plan-shape. Lifting line theory shows elliptic loading to cause the lowest amount of induced drag, and provides the insight that in presence of a hull, the symmetry line of the vortex system of a lifting body placed normal to the hull lies at the hull, meaning that an optimal foil will have a span-wise distribution of chord-length that is a half ellipse with the semi-axis of the ellipse coinciding with the hull. Measurements in Pempraneerach, *et al.*, (2003) showed that to achieve low rotation moments on the fins, a chord-position of 33% is close to optimum. Consequently, a plan shape emerges, built of 2 ¼ ellipses that share a common largest semi-axis, and which is placed on the rotation axis of the fin, as illustrated in figure 5.

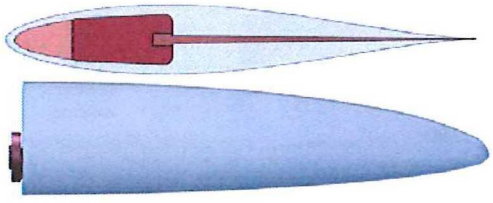

Figure 5: Generic plan-shape, chord shape and structure of fins. Aspect ratio will vary.

Chord-shape. From practical mechanical considerations, we need fins that are as strong as possible, and therefore have the largest thickness at the location of the rotation axis, which we know to be at 33% chord-length. A NACA 63015 chord-profile was selected for the fins with 15% chord thickness and a maximum thickness at 33% of chord-length, for a foil-profiles that is symmetrical, efficient, strong, and at the same time delays stall as much as possible.

Span-wise flexibility. The effect of span-wise flexibility on the fins was excluded from this study; the value of total span-wise deflection due to all elastic phenomena throughout the range of parameters averages 1.8% of stroke, with a std. deviation of 0.7%.

Chord-wise flexibility. Pempraneerach, *et al.*, (2003) measured a large positive effect on propulsive efficiency at Re=4.10^5 when introducing chord-wise flexibility in flapping fins. The flexibility value was linked to the shore-hardness of rubber material, with limited data on actual bending behavior.

Distribution of chord-wise flexibility. We decided to limit the scope of investigation to fins with chord-wise flexibility confined to the part downstream of the rotation axis. We could not easily picture chord-wise flexibility upstream from the rotation axis to improve efficiency: stored mechanical energy would always be restituted against the direction of motion, and the camber distribution would worsen. We could also not find any corresponding example in nature. The fins are designed in such a way that the ratio of chord-wise deflection to chord-length is constant along the span when a fin is placed perpendicularly to the flow. We finally decided to increase flexibility linearly from the rotation axis to the trailing edge by placing a spring with triangular section because:

- Bending would otherwise be concentrated close to the fin-rotation axis
- Increasing flexibility close to the trailing edge allows the stored mechanical energy to be released as a positive pressure field downstream when making the turn at the end of stroke
- Fish & Rohr (1999) demonstrated that such a chord-wise flexibility distribution seems to be implemented with sea-mammals and fish

Amount of chord-wise flexibility; characteristic fin pressure P_F. With the approach so far, it becomes natural to characterize a given fin by the dynamic pressure at which its chord bends a fixed percentage -- 10% -- when placed perpendicularly to a flow; we call this dynamic pressure the characteristic fin pressure P_F. Because a fin essentially has to bend to cause effect of chord-wise bending, it is reasonable to assume that the

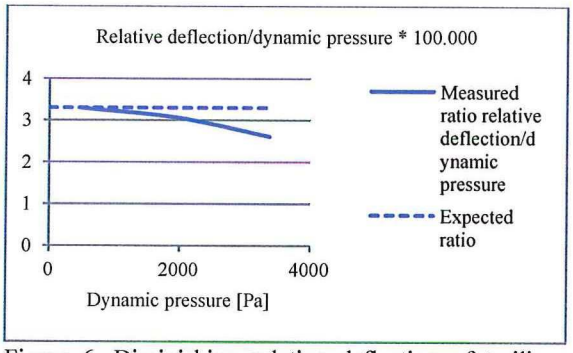

Figure 6. Diminishing relative deflection of trailing edge with increasing perpendicular dynamic pressure

dynamic pressure during the propulsion cycle and an efficient P_F are of the same order of magnitude. We define the dimensionless flexibility E_2 as $Peak\_dynamic\_pressure / P_F$:

$$E_2 = \frac{\rho(V_{advance}^2 + r^2\omega^2)}{2.P_F} \qquad (10)$$

E_2 behaves as a dimensionless flexibility number: if $V_{advance}$ increases or ω increases, E_2 goes up; the dynamic pressure will also increase, and chord-wise bending of the fin increases, which is equivalent to increased chord-wise flexibility. It seems reasonable to look for efficient values at $0.5 < E_2 < 2$. Several other definitions would be possible for E_2, but this one corresponds to deflection under propulsive loading.

Realization. The mechanical approach is to build the fins out of a rigid beam which also is the fin-stem, include a span-wise grove in the beam to fit a 3D milled spring with a chord-wise triangular section, and finally add a very flexible envelope to achieve the desired chord-shape. This is depicted in figure 5. The spring is designed for constant deflection-ratio at given dynamic pressure. The deflection of two fins with different characteristic flexibility P_F was measured at scale 1/12 under different dynamic pressures when placed perpendicularly to the flow. It was found that the utilized envelope material increases the P_F value by 1000 Pa compared to the calculated spring value, and that deflection/chord-length varies 10% along the span. Measurement of chord-wise deflection revealed that chord-wise deflection does not obey a linear relationship with dynamic pressure as one would expect from analytic mechanical analysis, but is less progressive. Measurement at 3 speeds yield an estimate for marginal chord-wise deflection at 10% bending to be 30% lower than close to 0% bending.

3. Performance predictor. Comparative map of losses for flapping propulsor & screw-propeller

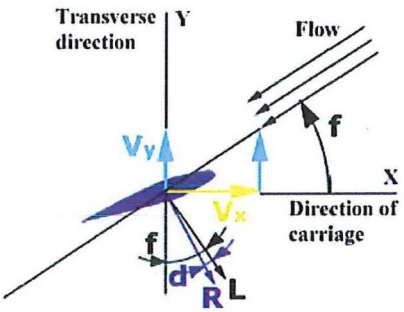

Figure 7: Reaction force, lift, flow angle and drag angle of a foil or a propeller blade element

General approach

We separate the losses in backwards kinetic energy losses (accounted for in the ideal efficiency) and downwash-induced and viscous energy losses (accounted for in the blade efficiency):

$$\eta_{open\ water} = \eta_{ideal} \cdot \eta_{blades} \qquad (11)$$

Actuator disk theory gives us the expression for ideal efficiency η_{ideal} and flow speed through the actuator as in (5) and (6), using the required thrust and the dimensions of the considered propulsor.

The blade efficiency η_{blades} embodies losses caused by downwash and viscosity. We can estimate η_{blades} in the same manner for all propulsors by a simple integration of the hydrodynamic reaction force, taking into account the flow-angle and the drag-angle of the foils. For a screw-propeller, flow-angle and drag angle vary with radius, and do not vary in time in open water conditions and we integrate the reaction force along the radius. For a flapping-propeller the flow-angle and drag angle vary in time, but can be estimated for the whole fin using lifting line theory, and we integrate the reaction force along the cycle.

In open water conditions, the propulsor is attached to a carriage that replaces the ship. Each fin or blade element sees:

- A reaction force $\vec{R}$ at a given drag angle (d) with the lift force $\vec{L}$ normal to $\vec{V}_{flow}$ at flow angle (f)
- An instantaneous speed $V_y\vec{j}$ relative to the carriage.
- And propels the carriage moving at $\vec{V}_{carriage}$, seeing a forward flow speed $V_x > V_{carriage}$ due to kinetic energy losses
- We approximate $||\vec{R}|| = ||\vec{L}||$, which is equivalent to assuming that (d) is small

By projection:
$\vec{R} = R.\sin(f-d).\vec{\imath} + R.\sin(f-d).\vec{\jmath}$
Power input to the fin: $E_{in} = \vec{R}.V_y\vec{j}$
Power output by the fin: $E_{out} = \vec{R}.\vec{V}_{carriage}$

Actuator disk theory gives:
$$\vec{V}_{carriage} = V_x.\eta_{ideal}.\vec{\imath} \qquad (12)$$

We express the local efficiency of the blade element:
$$\eta = \frac{E_{out}}{E_{in}} = \frac{\vec{R}.\vec{V}_{carriage}}{\vec{R}.V_y\vec{j}} = \frac{R.V_x.\sin(f-d)}{R.V_y.\cos(f-d)}\eta_{ideal}$$
$$\eta = \frac{V_x}{V_y}\tan(f-d)\eta_{ideal} = \frac{\tan(f-d)}{\tan(f)}\eta_{ideal} \qquad (13)$$

Taking into account the fact the reaction force flips when the flow angle changes sign:

$$\eta = \frac{\tan(|f|-|d|)}{\tan(|f|)}\eta_{ideal} = \eta_{blade}.\eta_{ideal} \qquad (14)$$

For a screw-propeller, the flow angle (f) varies with distance from hub, and for a flapping propeller the flow angle (f) varies with time.

Efficiency map of the design screw-propeller

Applying this approach to the design propeller of the selected container feeder, we split the losses in blade losses and ideal losses, and we map the local efficiency of the propeller section radially.

Using (14):
$$\eta = \eta(r) = \frac{\tan(|f|-|d|)}{\tan(|f|)}\eta_{ideal}$$

Actuator disk theory provides:
$$C_T = \frac{T}{½\rho¼\pi D^2 V_{carriage}^2}\ ;\ \eta_{ideal} = \frac{2}{1+\sqrt{1+C_T}} \qquad (15)$$

Using propeller data of the feeder as given in table 1:
η_{ideal} = 87% (C_T = 0.70)
η_{blades} = 72% = $\eta_{openwater}/\eta_{ideal}$

Immediate geometric consideration, and substitution using (12) gives the flow angle for the screw-propeller:

$$\tan(f) = \frac{\omega.r}{V_x} = \frac{\omega.r.\eta_{ideal}}{V_{carriage}} = \frac{\pi.\eta_{ideal}}{J.R}r \qquad (16)$$

A stepped approach with explicit hypotheses yields the drag angle:

Chord-length distribution: ½ ellipse. This yields the radial chord distribution c(r) from the known surface and dimensions.

Circulation distribution: ½ ellipse. Knowing J gives the flow angle distribution according to (16). This in turn allows us to predict the lift force and to obtain the radial thrust distribution T(r) and total thrust T based on any maximum value of circulation using:

$$L(r) = \rho.V(r).\Gamma(r) \quad (17)$$

We calculate the needed correction of thrust and apply it to scale circulation, and recalculate lift distribution and then thrust distribution. The lift coefficient is:

$$C_L(r) = \frac{2.\Gamma(r)}{c(r).V(r).\Delta r} \quad (18)$$

C_L is used to estimate the induced of drag using: $C_D(r) = C_{d0} + C_L^2(r)/\pi AR_{blade}$, and calculate C_{d0} to match the measured performance η_{blades}= 72%.

We obtain: C_{d0}=0.009 which is realistic, Γ_{max}=2.65 m^2/s, C_{Lmax}=0.12, average L/D=9.5 causing average drag angle d=6.1 deg with a flat distribution.

We now have the drag angle distribution d(r). We already had the flow angle distribution f(r). This allows us to plot the estimated thrust distribution and local blade efficiency of the screw-propeller as a function of the radius (figure 11) and as a function of the flow angle (figure 8).

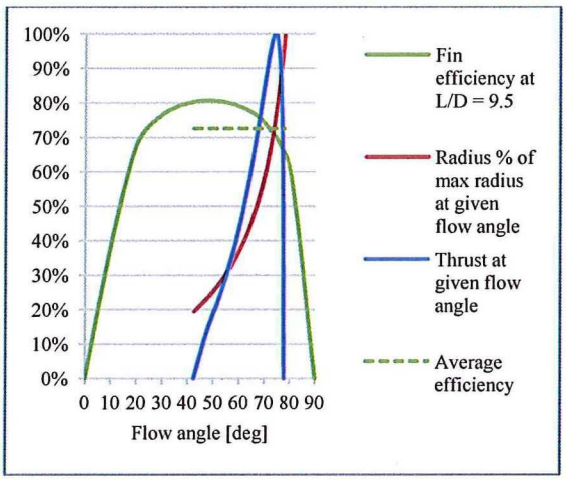

Figure 8: Approximate distribution of thrust and blade efficiency according to flow angle for the screw-propeller of the container feeder

The locus of high thrust of the screw does not coincide with the locus of high efficiency. The thrust density peaks at 70 degrees flow-angle approximately, which is far removed from the optimal 45 degrees angle. To be optimal in terms of flow-angle, a screw propeller would have to operate at $J \approx 70\%\pi$, when the locus of maximum thrust density operates at 45 degrees flow-angle (see figure 8).

Open-water efficiency map of the flapping propulsor and quantification of unsteady effects

Applying the same approach to a near optimal flapping propulsor for the selected container feeder, we again split the losses in blade losses and ideal losses, and we map the efficiency of a flapping fin as a function of phase angle in the cycle. Again, the flow-angle is simple to calculate using the advance ratio J. Thrust and drag angle must be estimated carefully.

Theodorsen (1935) showed 2 effects on the lift force of a foil in case of cyclical heave & pitching:

- Addition of a term in the direction of heave equivalent to an added mass effect on the fins. This term does not perform any work and does therefore not be taken into consideration for thrust and efficiency estimates.
- Lift reduction and lift delay compared to lifting line theory as a function of the reduced frequency $k = \pi.N.c/V$, where N is the frequency of heave, and where observed lift can be expressed by a complex vector as a function of Hankel functions that is represented in Figure 9.

Figure 9 shows that at least half of the ultimate steady-state lift is obtained for high frequencies of velocity fluctuations, and that lift is delayed within the cycle as reduced frequency increases. The phase delay for the lift is the angle of $C(k)$ on the graph. The highest delay is close to 16 degrees phase angle at $k = 0.2$. Delay displays limited variation for $0.2 < k < 0.6$, which corresponds to the range of the machine.

Figure 9 also shows that the expected lift reduction in the indicated range $0.2 < k < 0.6$ will be between 25% and 40%. This latter observation merits qualification. Although the lift is reduced compared to what would be a steady-state end-result, unsteady

Table 2. Parameter definitions for flapping propulsor

Number of fins	n	Hull-effect AR multiplier	h
Fin spacing on chariot	g	Stroke of flapping machine	D
Fin span	s	Phase lag of lift	φ_{lag}
Fin surface	S_{fin}	Unsteady Lift reduction	l_k
Fin plan-shape factor	e	Lift factor due to chord shape	l_r

propulsion delays stall, and the required average lift can be reinstated by increasing the average angle of attack. Increasing the angle of attack amounts to reducing the pitching angle. This increase of the average angle of attack does not come at the expense of higher induced drag (no increase in downwash) or higher viscous drag (no increase in speed). Some increase in pressure drag may be expected however.

Taking the aforementioned considerations into account, for the assembly of a first order estimator for thrust & efficiency, we utilize a quasi-steady approach with lifting line theory and project and integrate forces on sufficiently short time steps, while introducing 15 degrees delay in the lift force and a lift reduction of 35% that is compensated by a reduced pitching amplitude corresponding to an increase in angle of attack for the same lift coefficient.

Using (14), we map the losses of the flapping propulsor in time instead of in space:

$$\eta = \eta(t) = \frac{\tan(|f| - |d|)}{\tan(|f|)}\eta_{ideal}$$

Actuator disk theory and geometric consideration give:

$$\eta_{ideal} = \frac{2}{1+\sqrt{1+C_T}}$$

$$C_T = \frac{T}{½\rho.(D+(n-1)g).s.V_{carriage}^2} \quad (19)$$

We use approximation (8) for the needed expression of the flow angle, where we have J as an input variable.

$$f(t) = Atan\left(\frac{\pi.\eta_{ideal}}{J}\sin(\omega t)\right) \quad (20)$$

For the drag angle of the fin, we calculate its lift and drag coefficients. For the lift coefficient, we use thin airfoil approximation corrected for lift reduction due to unsteady effects, corrected for a chord profile with non negligible thickness, and corrected for phase lag, and apply it to the expression of angle of attack (9):

$$C_L(t) = 2\pi l_k l_f\left(Atan\left(\frac{\pi.\eta_{ideal}}{J}\sin(\omega t - \varphi_{lag})\right) - Atan\left(\frac{\pi}{J_c}\sin(\omega t - \varphi_{lag})\right)\right) \quad (21)$$

The drag coefficient, using lifting line theory with a correction factor for hull effect, and a parabolic factor f_{C2D} for increase in 2D turbulent drag of the profile, is:

$$C_D(t) = C_{d0} + C_L^2(t)\left(\frac{1}{\pi.e.h.AR} + f_{C2D}\right) \quad (22)$$

The expression of the instantaneous drag angle is then:

$$d(t) = \text{atan}(C_D/C_L) \quad (23)$$

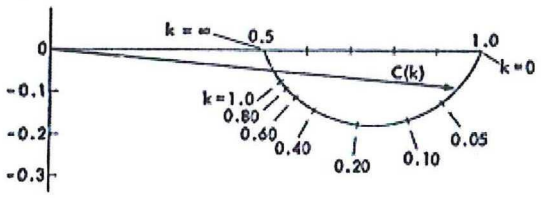

Figure 9. Reduced and delayed lift C as a function of reduced frequency k

We then express the instantaneous thrust of the fin while separating fixed and time-varying terms:

$$T(t) = \frac{n\rho S_{fin}V_{carriage}^2}{2\eta_{ideal}^2}.\frac{C_L.sin(|f|-|d|)}{cos^2(f)} \quad (24)$$

The average thrust is calculated by integration over one cycle. The instantaneous efficiency is already known (14), and the average efficiency is calculated by integrating thrust weighed efficiency over a cycle.

Optimizing input variables for performance of the flapping propulsor, we obtain we obtain the dataset depicted in table 3, with a very high predicted open-water efficiency of 87%. We chose $J=\pi$ to operate closely to the highly efficient 45 degree flow-angle. Figure 11 presents the calculated efficiency and thrust distribution for the flapping propulsor of the selected container feeder as a function of phase angle.

Table 3. Input and result of lifting-line performance model of the flapping propulsor of the selected ship

Fixed parameter values for the lifting-line performance model			
Machine parameters		Chord-shape data at Re=10^7	
Stroke D	4.753 m	NACA profile ref	63015
Fin distance g	1.43 m	C_{d0}	0.01
Number of fins n	6	f_{C2D}	0.01
Fin span	5.62 m	l_f	0.9
Hydrodynamic parameters		Unsteady parameters	
Plan shape factor e	1	φ_{lag}	15 deg.
Hull-effect h	2	l_k	0.65
Input values for the lifting line performance model			
Critical advance ratio J_c	4.64	Needed thrust	800 kN
		Speed	10.13 m/s
Advance ratio J	π	Fin surface S_{fin}	6.09 m^2
Result of the lifting-line performance model			
Frequency N	0.67 Hz	Av. chord length	1.08 m
Maximum instantaneous thrust	1600 kN	Fin AR	5.18
		C_{Lmax}	0.6
Maximum lift-force per fin	402 kN	$\alpha_{attack\ max}$	9.4 deg
		Average Lift/Drag	24
Blade efficiency η_{blade}	92.2%	Flow angle f_{max}	43.5 deg
		Fin angle $\alpha_{fin\ max}$	34.0 deg
Reduced freq. k	0.22	Thrust coeff. C_T	0.23
Result of actuator disk theory			
Ideal efficiency η_{ideal}		94.8%	
Open water eff. $\eta_{open\ water}$		87.4%	

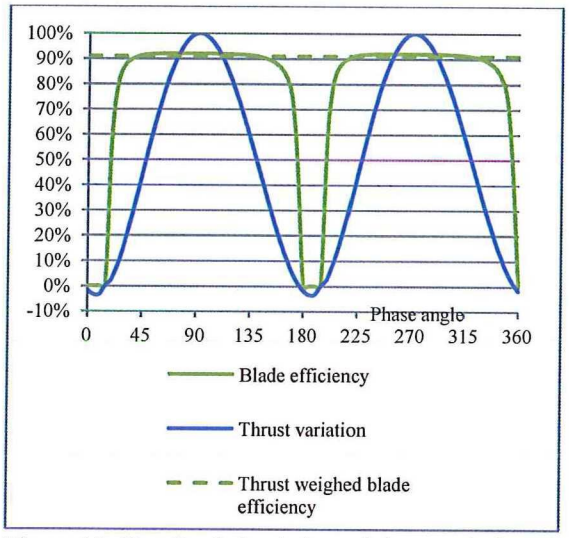

Figure 10: Result of simulation of time evolution of thrust and efficiency for a the flapping propulsor of the container feeder for the chosen parameters at 800 kN thrust, V=10.13 m/s and J=π

Concluding comparison between screw-propeller and flapping propulsor using lifting line theory on the case of a container feeder

Table 4 shows that the flapping propulsor opens the perspective of much improved efficiency compared to a screw-propeller. Although the gain in ideal efficiency of the flapping propulsor is an appreciable 8%, its largest gain potential is projected to come from better blade efficiency, where the gain is 19%. Strengths of the flapping propulsor are:

- A larger actuator area that reduces impulse losses
- Having high thrust and high efficiency coincide in time, whereas the locus of high efficiency and high thrust density do not coincide for the screw-propeller as fig. 10 & 11 show. This is the price the screw-propeller pays for high thrust density.
- High AR foils & hull effect, resulting in low induced drag
- Lower flow speed, resulting in more efficient flow-angles, and in lower viscous losses due to possibility for higher lift coefficients

Table 4. Components of open-water efficiency for both propulsor-types at proper thrust and speed

	Screw	Flapping
Open water efficiency $\eta_{openwater}$	0.63	0.86
Ideal efficiency η_{ideal}	0.87	0.95
Blade efficiency η_{blades}	0.72	0.91

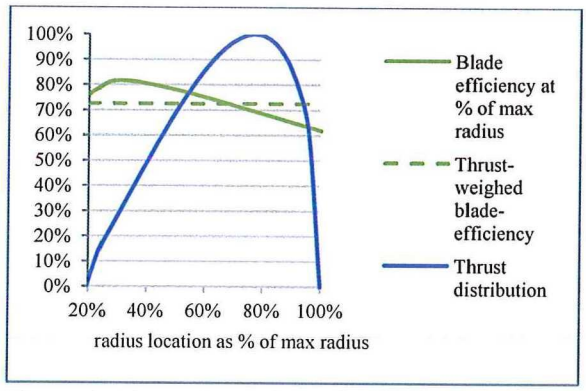

Figure 11: Approximate thrust distribution and blade efficiency distribution of the screw-propeller of the selected container feeder according to radius

4. Measurement approach and uncertainty analysis

Experimental set-up and assessment of systematic measurement bias

This research program measures the practical potential of open-water efficiency of flapping propulsion. Effects relating to propulsor/hull interaction were therefore to be eliminated, as were effects of mechanical losses of the propulsor. Because the near-optimal flapping propulsor needs a submerged surface to operate against, and to avoid potentially substantial free surface effects, the propulsor was placed on a flat barge of sufficient dimensions (2 times actuator width) with 2 mm immersion, with submerged fins following the flat surface with their rotation axis perpendicular to the barge surface. The result is a propulsor operating in a uniform flow. Fig. 12 shows the general test lay-out both under and above water.

The propulsor includes a sliding/rotating seal between the machine and the water. Due to the objective of neutralizing mechanical losses in the measurement program, it was decided to place custom-built transducers between the fin-stems and the source of motive motion at the fin-root, while avoiding contact with the seal-elements to preclude interference

Figure 12: Test set-up of flapping propulsor

of forces stemming from the dynamics of the seal. These transducers, depicted in Figure 13, operate in the reference system of the fins and allow to measure the instantaneous values of needed forces. Figure 14 represents the utilized signal-processing workflow.

To determine a representative efficiency of flapping propulsion, the characteristics of the servo-drive were matched to the actual constant torque behavior of a typical diesel prime-mover during the propulsive cycle. To that effect, the control logic of the servo-drive was configured to change signal intensity only at each extreme translation positions of the fins. In this manner, in-cycle fluctuations of the rotational speed of the driving-shaft of the flapping machine are essentially identical to those that would be observed at full-scale in an actual ship, and these fluctuations are determined by the energy absorption pattern of the fins and the changes in internal kinetic energy. Data on the actual level of in-cycle speed-fluctuation of the drive-shaft is presented in the analysis of the measurements. The effect of varying that fluctuation level through variation of the moment of inertia of the flywheel is also shown.

The tests were performed in MARIN's Depressurized Towing Tank, measuring 240x18x8m. The large width and depth of this basin ensures a negligible blockage effect. A 15 min. pause between measurements ensured absence of remaining eddies in the water of the tank.

The Reynolds number over the fins was kept above 2.10^5 to avoid laminar flow over the fins, and the leading edges were roughed according to ITTC prescription and MARIN practice. This caused the need to perform measurements at a scale $1/12^{th}$ or larger, resulting in a sizeable machine (2m wide with 396mm stroke) of the selected 150 m ship.

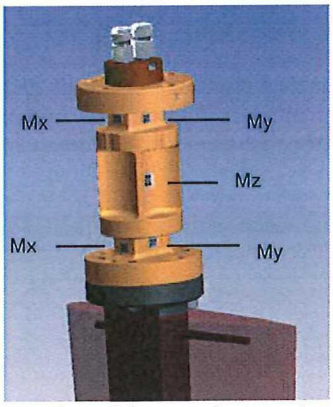

Figure 13: Location of the transducer and strain gauges

Measurements lasted on average 47 completed stable cycles for precision. Approximately 10% of the measurements have been performed twice while switching transducers in order to assess repeatability. The measurement program was designed in such a way that values of representative non-dimensional variables were varied in isolation of each other as much as possible to make trends and dependencies visible.

Logging of all dynamic variables including forces, moments, angles of fins, and crankshaft angle and systematic logging of measurement parameters generated a retrievable trail of time-data and associated parameters. Computational approach for derived values such as input power or efficiency, and scaling approach to forces and efficiency were designed for absence of bias, and are described in the preceding paragraphs, including a consideration on accuracy.

Conclusion on risk of systematic bias in the presented experimental results: The program complies with common best practices in towing tanks experiments. Design also shows that measurement bias has been avoided in all areas that we understand with present knowledge, and that measurement bias in the program is probably of an order of magnitude smaller than stochastic incertitude.

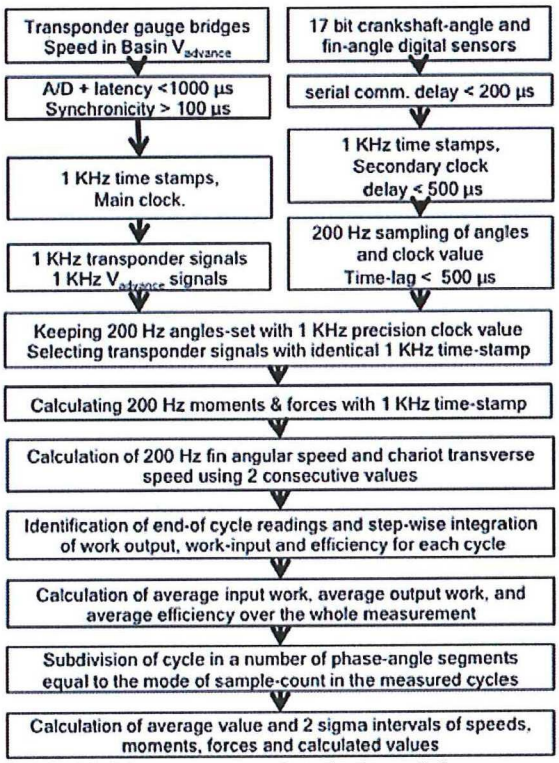

Figure 14. Measurement and analysis workflow

Instrumentation, calibration and accuracy

The aim of the design of the experimental set-up and instrumentation was to measure only the forces and efficiency on the fins. To enable this, a transducer is needed that could be connected directly to the fin, and that could measure moments and forces along all axes. The optimum position of this transducer would be on the location where the forces and moments are acting (approximately in the middle of the span of the fin, about 20 cm below the stem). The needed size of the transducer and the requirement of easy exchange of fins led to the decision to place the transducer at the root of the fin (see fig. 13).

This location will lead to relatively high moments in x and y directions. Based on these considerations, it was decided to design a 5-component transducer, which measures Mx at two locations, My at two locations and Mz. Fig. 13 shows the locations of the various strain gauges. The strain gauges measuring the bending moments in x, y and z directions are indicated. The distance between the upper and lower strain gauges is 0.055 m. With the convention that subscripts t and b stand for top and bottom, the forces in x and y-direction are calculated by:

$$Fx = \frac{(My_t - My_b)}{0.055} \qquad Fy = \frac{(Mx_t - Mx_b)}{-0.055} \quad (25)$$

During the oscillation of the fin, the forces in y-direction will be much larger than the forces in x-direction. This will lead to a relatively large signal from the Mx strain gauges, while the signal from the My strain gauges will be low. In order to obtain the largest possible signal (and highest accuracy) in both x and y directions, the signal from the My gauges has been increased by weakening the transducer in that direction. This led to an asymmetric element (fig. 13), with maximum loads as indicated in table 5.

Due to limited available space between the root of the fin and the Finprop driving system, the transducer had to be kept as small as possible. The various strain gauges are therefore located very close to each other. This leads to interactions between the strain gauges

Table 5: Maximum loads per component

	Maximum load per component	Unit
Fx	2000	N
Fy	3000	N
Fz	10000	N
Mx	110	Nm
My	77	Nm
Mz	28	Nm

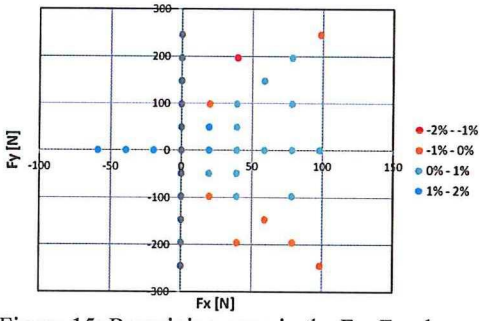

Figure 15: Remaining error in the Fx, Fy plane of a transducer after calibration

when a force is applied at a certain distance below the transducer as confirmed by initial checks.

Based on this insight a calibration program was developed, in which the transducer was calibrated in the Finprop machine and where combined forces were applied at various distances below the transducer. A total of 224 tests per transducer have been conducted. In this case five strain gauges are present which can interact with each other. So, equation (25) needs to be expanded with the contribution of other strain gauges. In case of a linear system, the relation between Fx, Fy, Mx, My and Mz and the output of the strain gauges can be formulated as a matrix operation:

$$\begin{pmatrix} Fx \\ Fy \\ Mx \\ My \\ Mz \end{pmatrix} = \begin{pmatrix} a_{11} & a_{12} & a_{13} & a_{14} & a_{15} \\ a_{21} & a_{22} & a_{23} & a_{24} & a_{25} \\ a_{31} & a_{32} & a_{33} & a_{34} & a_{35} \\ a_{41} & a_{42} & a_{43} & a_{44} & a_{45} \\ a_{51} & a_{52} & a_{53} & a_{54} & a_{55} \end{pmatrix} * \begin{pmatrix} Mx_t \\ Mx_b \\ My_t \\ My_b \\ M_z \end{pmatrix} \quad (26)$$

Adequate calibration matrices were obtained by multi-variable regression with linear terms and two cross terms. Residual errors in Fx and Fy appeared to be ± 2%. The calibration program proved the magnitude of hysteresis, when going from zero strain to the maximum value and back to zero, to be limited to about 0.1% per cent of the maximum load, or 2N. This 2N value can be considered good, but could nevertheless influence measurements with low average readings. In figure 15 an example of the error in Fx is given of one of the transducers for a number of applied combinations of Fx and Fy.

Time-stamping, time accuracy

As Figure 14 shows, interfacing between the towing tank measurement infrastructure and the independently engineered flapping propulsor caused a need for two synchronized clocks: the towing-tank clock with which carriage speed and transducer data were read, and the propulsor clock with which fin-

angles and chariot positions were read. Latencies and synchronization offsets in the two paths are shown in figure 14. The approach results in a dataset at 200 Hz with 0.1 ms synchronous force & moment measurements, with 1.2 ms max. time-lag between fin-angle & crankshaft-position on one hand and moments & forces on the fins on the other hand. On an average period length of 600 ms in the program, the maximum synchronicity error represents a phase delay of 0.7°.

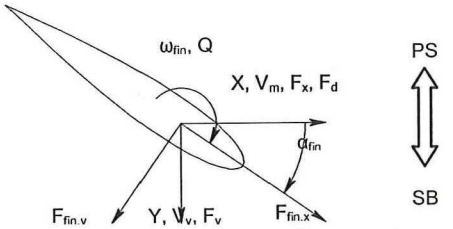

Figure 16: Representation of forces acting on the fin.

Accuracy of thrust and delivered power

The force transducers rotate with the fin. To compute the absorbed power and the delivered power, the projected forces are needed in longitudinal and transverse direction with respect to the ship:

$$F_x = F_{fin,x}.\cos(\propto_{fin}) - F_{fin,y}.\sin(\propto_{fin}) \quad (27)$$

$$F_Y = F_{fin,y}.\cos(\propto_{fin}) - F_{fin,x}.\sin(\propto_{fin}) \quad (28)$$

Where $F_{fin,x}$ and $F_{fin,y}$ are the chord-wise force and perpendicular force on the fin. Figure 16 gives a schematic representation of the forces acting on the fin. The delivered thrust over a cycle is then computed as the stepwise time-integration of F_x and the absorbed power over a cycle is then computed as the stepwise integration of F_x . $V_{advance}$:

$$T = \frac{1}{T}\sum_{i=1}^{end\ cycle} F_{x,i}.\Delta t_i \quad (29)$$

$$P_D = \frac{1}{T}\sum_{i=1}^{end\ cycle} F_{x,i}.V_{advance,i}.\Delta t_i \quad (30)$$

We have seen the transducer signals to have 2% uncertainty, and we will show this to be the main contributor to uncertainty for thrust T and absorbed power P_D. We reduce the uncertainty analysis to first order uncertainty effects only.

The precision of $V_{advance,i}$ is 0.1% or better and near-constant; the same holds for the precision of Δt_i which is dictated by a high-quality clock. The accuracy of the delivered power is therefore dominated by the average accuracy of delivered instantaneous thrust $F_{x,i}$ and its rate of change.

We may neglect the impact of the rate of change of $F_{x,i}$ on the accuracy P_D: with on average 600 ms cycle periods and a 5 ms sampling interval during the program, the average phase-angle step per data-sample is 3°, resulting in 2.5% [=sin(3°)/2] max inaccuracy for a single data-point given a harmonic approximation for $F_{x,i}$. This 2.5% inaccuracy almost vanishes over the cycle average due to the substantial Y-axis symmetry around the mid-stroke maximum per ½ cycle and monotonic behavior per ¼ cycle (Fig 29): systematic bias in the 1st ¼ cycle is largely offset by systematic bias in the 2nd ¼ cycle. We also neglect the effect of the max. 0.7° phase delay between measured forces and measured angles as discussed in the time-stamping paragraph for the same reason.

The deviation map of the transducers (figure 15) shows that we cannot expect cancellation when F_y changes sign and F_x keeps its sign throughout a cycle. We approximate the imprecision of thrust T and delivered power P_D to be equal to the average measurement error of the transducers. This results in an estimated 2% accuracy of T and P_D either over a period or over the entire measurement run. This result is confirmed by repeatability tests within 2%, the smooth shape of the curves displayed in subsequent paragraphs, and the narrow 2σ bands as seen in fig. 29.

Accuracy of absorbed power

With Q the moment required to rotate the fin, ω_{fin} the angular speed of the fin, and V_y the transverse speed of the fin, the absorbed power per fin becomes:

$$P_A(t) = -F_y.V_y - Q.\omega_{fin} \quad (31)$$

$$P_A = -\frac{1}{T}\sum_{i=1}^{end\ cycle} (F_{y,i}.V_{y,i} + Q_i.\omega_{fin,i}).\Delta t_i \quad (32)$$

In expressions (31) and (32), translation speed V_y and the angular speed ω_{fin} are computed as the rate of change of α_{fin} and as the rate of change of the chariot-position between two consecutive datapoints. Defining α_c as the crankshaft angle, equal to the phase angle with the conventions of chapter 1, we compute:

$$\omega_{fin,i} = (\alpha_{fin,i+1} - \alpha_{fin,i})/\Delta t_i \quad (33)$$

$$V_{y,i} = \frac{\cos(\alpha_{c,i+1}) - \cos(\alpha_{c,i})}{\Delta t_i}.R_{crankshaft} \quad (34)$$

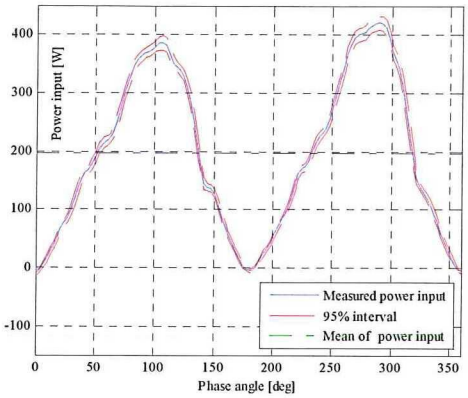

Figure 17: Absorbed power & 95% uncertainty interval

As in the paragraph for delivered power, we limit accuracy analysis to the addition of first order uncertainty effects, and we use similar reasoning. Table 8, line 16 shows us that the average fin-rotation power is less than 1% of total power over a cycle. Therefore, inaccuracy of the term $Q_i.\omega_{fin,i}$ in expression (32) of absorbed power, corresponding to fin rotation, can be fully neglected. We are then left with a similar expression for absorbed power as for delivered power, except for the fact that $V_{y,i}$ is computed as in (34) rather than directly measured.

Computing of $V_{y,i}$ as in (34) introduces noise because of the uncertainties described in the paragraph on time-stamping: we introduce a 1 ms uncertainty on both sides of a time-segment of length 5 ms. Table 8, line 1 gives us an average count of cycles of 47 throughout the program, and the central limit theorem tells us that the value of the mean of the samples at each phase-angle location converges towards the value of the mean of the measurements. Fig. 18 displays the observed scatter of readings for absorbed power, and we see a 2σ interval of approximately 15%. With 47 datapoints at each phase-angle position, uncertainty on the mean time-values is 2% ($= 0.15 / 47^{0.5}$), with a 95% probability.

The calculated 2% uncertainty on transverse speed $V_{y,i}$, and a 2% uncertainty over the measurements of $F_{y,i}$, obtained in the same manner as for delivered power P_D, result in 2.8% uncertainty on absorbed power $\overline{P_A}$ over a measurement run [$= (2^2 + 2^2)^{0.5}$].

Accuracy of open-water efficiency

Due to the fact that absorbed power needs a full-run to be reliably measured and computed, the computed open water efficiency must be computed over a full run as well:

$$\bar{\eta}_{OA} = \bar{P}_D / \bar{P}_A \tag{35}$$

An assessment of uncertainty of open-water efficiency computations follows directly from the previously made assessments of uncertainty of the numerator, at 2%, and of the denominator, at 2.8%. The uncertainty of open water efficiency computations is then 3.5% [$= (2^2 + 2.8^2)^{0.5}$]. This value is consistent with repeatability tests that were always observed to be within 2%, and with the well-behaved patterns of curves obtained in subsequent sections.

Accuracy of fin frequency

Measurement of frequency does not play a role in the computations of absorbed, developed power, or open water efficiency, but is better than 1%.

Changes in rotational speed due to variations in kinetic energy of the system at different points of the cycle will affect the cycle of angle of attack. Speed variations of the drive-shaft show-up in a FFT of the angular position signal. Table 8, line 4 shows that 95% (2σ) of the measurements have been performed with less than 1.2% speed variation, which is equivalent to 0.3 degree variation in angle of attack approximately, or 2.5% of the average angle of attack.

Uncertainty due to scaling method

To obtain the results on full-scale, corrections have been made for scale effects on the friction due to the difference in Reynolds number at model scale and full scale. The Reynolds number is calculated using the average chord length and the total inflow velocity defined as:

$$V_t = \sqrt{V_{advance}^2 + V_y^2} \tag{36}$$

The friction coefficient for model scale has been calculated using the Katsui friction line:

$$C_f = \frac{0.0066577}{(\log_{10} Re - 4.3762)^{0.042612 \log_{10} Re + 0.56725}} \tag{37}$$

For the full-scale Reynolds number, the friction coefficient cannot decrease below the roughness-dominated friction coefficient, which is computed with the Prandtl-Schlichting formula:

$$C_R = \left(1.89 + 1.62 \log_{10}\left(\frac{c}{e}\right)\right)^{-2.5} \tag{38}$$

with the roughness e taken as 30 μm. The form factor is computed with the ITTC 78 formula:

$$(1 + k) = 1 + 2\frac{t_{fin}}{c} \tag{39}$$

Where t_{fin} is the thickness of the fin. The 1+k value obtained for these fins was 1.30.

It is realized that the described scaling method neglects the induced velocities for the determination of the Reynolds number and scale effect correction. The decision was made to utilize the vector summation of ship speed and transverse fin speed for the Reynolds number because the effect of the approximation is not noticeable at this level of precision. Table 8, lines 12 & 13, show that the effect of scaling on efficiency is modest at **1-** 77.6/74.3 = 4.4%, and the scaling effect on thrust is calculated at 1 - 0.171/0.162 = 5.5%. A potential discussion on various approaches to Reynolds scaling can therefore not invalidate the conclusions from this study. We neglect this uncertainty in the overall uncertainty assessment.

Conclusions on uncertainty

Well-behaved curves in the sections 5 and 6 ahead, repeatability of results within 2%, a disciplined and documented approach to the design of the experimental set-up and to the structure of the measurement program, lead us to conclude that the results of this study should be reproducible. We can also conclude from the previous sections that increasing the sampling frequency will not improve measurement uncertainty, and that the main bottlenecks for higher accuracy are transducer precision and sampling/clock synchronicity. A summary of uncertainty on main results can be found in table 6.

Table 6. Summary of uncertainty levels

Item	**Uncertainty**
Transponder forces and moments	2%
Thrust over a cycle	2%
Thrust over a measurement run	2%
Power delivered over a cycle	2%
Power absorbed over a measurement run	2.8%
Efficiency over a measurement run	3.5%

5. Results: open water measurement set

Table 7. Data common to all measurements

Scale	1/12
Design speed	10.13 m/s
Stroke	D = 0.396 m
Fin span	0.468 m
Chord-shape	NACA 63015
Plan-shape	2x¼ ellipse as in figure 5
Rotation point	33% chord
Clearance of fin with immobile surface	0.001 - 0.002 m
Roughness	Leading edge roughness according to ITTC 1978 procedure to ensure turbulent flow
Sampling frequency	200 Hz with 0.1 ms synchronicity

Table 8. Statistics over the complete set of data, n=304

		Mean	Std dev.
1	Number of cycles measured	47	11
2	Advance speed	2.123 m/s	0.526 m/s
3	Flapping frequency	1.757 Hz	0.253 Hz
4	Largest peak of FFT of rotational speed	0.6%	0.3%
5	Reduced frequency k	0.31	0.17
6	Advance ratio J	3.09	0.89
7	Critical advance ratio J_c	4.93	1.15
8	Maximum fin angle = atan(π/J_c)	33.6 deg.	6.6 deg.
9	Estimated max. angle of attack	11.6 deg.	4.5 deg.
10	C_T as measured	0.162	0.224
11	C_T scaled	0.171	0.232
12	Measured open water efficiency	74.3%	15.2%
13	Open water efficiency scaled	77.6%	16.1%
14	Peak-thrust /Thrust	2.6	0.4
15	Peak-reaction-force / Thrust	3.8	0.9
16	Pitching-power / Total-power	0.5% median, 23% max	
17	Peak-pitching-torque / (Chord-length*Thrust)	0.37	0.14 [fat tail]
18	Flexibility number E_2	1.11	0.5
19	Average chord-length/stroke c/D	0.268	0.069
20	Estimated C_{Lmax}	0.64	0.15
20	Reynolds	$2.5\ 10^5$, lowest $1.8\ 10^5$	

The measurement program aimed at finding the best parameters for flapping propulsion for the case of the selected container feeder. The unknown hydrodynamic parameters consisted of all combinations of design and operational parameters: Advance ratio, critical advance ratio, chord-wise flexibility, chord-length, fin spacing. Little data was available to point toward the right combinations. Systematic coverage of all combinations in stepped values for such a large number of variables is unachievable. We chose to focus on the required value of non-dimensional thrust C_T as defined in (5) for the whole propulsor, and endeavored to get the best possible results in that vicinity by quantifying the main effects as independently as possible. The required C_T for the whole propulsor was designated the "reference C_T value" and not the required C_T value because the C_T per fin will likely not be the same as the C_T for the whole propulsor. Furthermore, changes in design for the machine will easily lead to a different value of C_T.

Efficiency and thrust of a single, rigid, high AR fin

Figure 18 shows the result of 3 test series that provide an overview of performance at several advance ratios J for 3 values of the critical advance ratio J_c. J_c is related to the maximum rotation angle of the fins through $atan(\pi/J_c)$. The measurements showed a higher efficiency than the benchmark value set by the open-water performance of the existing design screw-propeller, but the measurements also showed a higher load-sensitivity. Decreasing J_c by increasing the pitching angle results in an improved efficiency at the

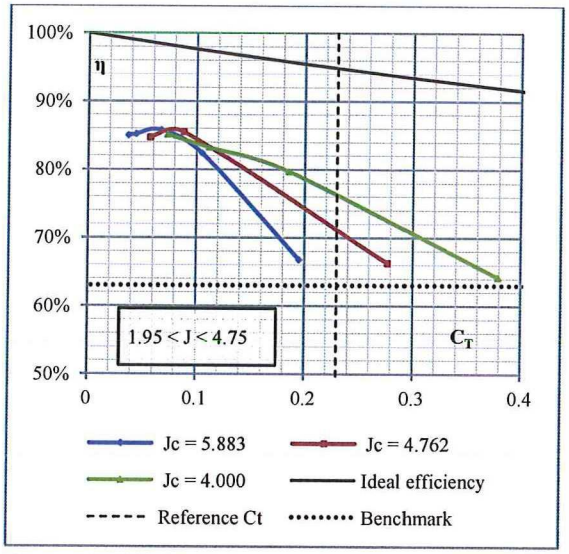

Figure 18. Efficiency versus non-dimensional thrust C_T of a single rigid fin with AR = 5.2, *Average–chord / Stroke* = c/D = 0.228 at three values of J_c

reference C_T. Existing measurements translate in an attainable open-water efficiency with a high AR rigid fins of 77%, with a possibility for slightly better results if we decrease J_c even further.

Efficiency and thrust of a single, flexible, high AR fin

The dimensionless flexibility number E_2 defined in (10) correlates well with thrust reduction

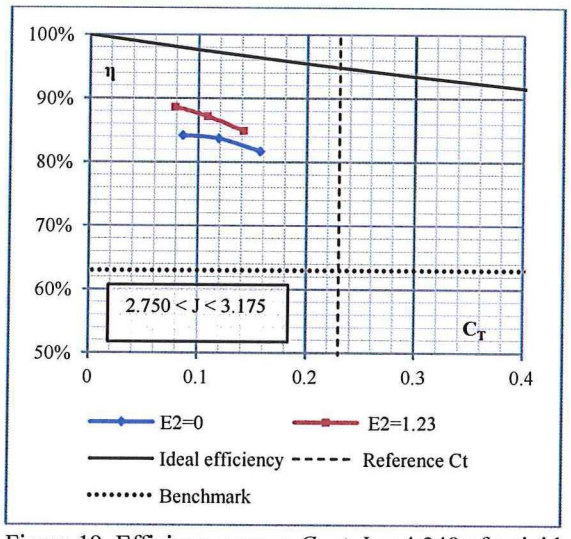

Figure 19. Efficiency versus C_T at J_c = 4.348 of a rigid fin and a flexible fin at constant flexibility number E_2; c/D = 0.228, AR = 5.2

Table 9. Thrust of rigid fin versus flexible fin with AR=5.2, c/D= 0.228, J_c = 4.348

J	3.18	2.95	2.75
C_T at E_2=0 (rigid)	0.088	0.121	0.161
C_T at E_2=1.23	0.081	0.110	0.144
Ratio $C_{T\ rigid}/C_{T\ flex}$	1.09	1.10	1.12

due to chord-wise flexibility on a few measurements where we could compare directly. Table (9) shows that the ratio C_{T_rigid}/C_{T_flex} of thrust coefficients of a rigid versus flexible fin varies only 3% when E_2, plan-shape and J_c are held constant at varying C_T. We defined the flexibility number E_2 in (10) as the ratio of maximum dynamic pressure to characteristic fin pressure P_F; a rigid fin would have E_2=0. A flexible fin, for a small angle of attack and a corresponding small deflection will have the same flexibility number as a larger deflection on a larger angle of attack. This notion of E_2 as a predictor of thrust reduction due to chord-wise flexibility would need further experimental validation.

E_2 as a measure for chord-wise flexibility does not appear to be a good predictor of efficiency gain due to chord-wise flexibility; if E_2 were a good predictor, figure 19 and 20 would have shown parallel curves.

A large number of measurements with the same plan-shape at various values of J_c and E_2 show that the efficiency effect of chord-wise flexibility increases with pitching-angle (lower J_c), and vanishes with loading. This is visible in figures 21 and 22. The magnitude of the positive effect of chord-wise

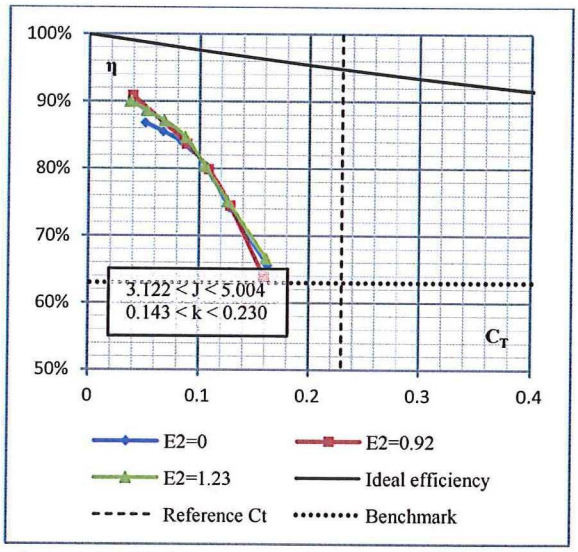

Figure 20. Efficiency versus C_T at J_c = 6.667 of a rigid fin and a flexible fin at constant flexibility number E_2; c/D = 0.228, AR = 5.2

flexibility however never seems very large with the *c/D* ratio that we tested. Curiously, although the efficiency of flexible fins falls faster with increasing thrust than for rigid fins at low C_T values, when increasing the loading further, the efficiency of the flexible fin never seems to fall below the efficiency of the rigid fin. This was observed at a broad range of J_c and *J*. No comparative data is available for efficiency and thrust of flexible versus rigid fins for $c/D \neq 0.228$.

Effect of fin-pitching range

The pitching range of the fin is related to the critical advance ratio by $atan(\pi/J_c)$. Figure 21 shows that a decrease in J_c increases efficiency at higher C_T, but reduces maximum efficiency slightly.

With $J_c = 2.95$, measurements show an open-water efficiency of 81% with the reference $C_T = 0.23$ for the container-feeder. This is a significant improve-

-ment of 22% of the flapping propulsor compared to the design propeller at proper loading.

Interpolation in the database at 81% efficiency yields an advance ratio $J = 2$, which results in a frequency at model scale of 3.7 Hz, which in turn results in a peak transverse acceleration of 107 m/s^2 ($\frac{1}{2}D\omega^2$) for the fins either in the model or at full scale. Such high acceleration is impractical for a full-scale machine with large dimensions. We must consequently seek for a lower C_T through a larger actuator surface or we must seek to decrease the transverse acceleration. The latter can be done through a combination of a larger crankshaft diameter, more fins, a larger single-fin-surface, or a higher J_c. Returning to the focus of this paragraph, future measurements should address the relative scarcity of measurements we have around the most attractive values for the container feeder at J_c = 2.75, 3.15 and 3.35 for this specific ratio *c/D*.

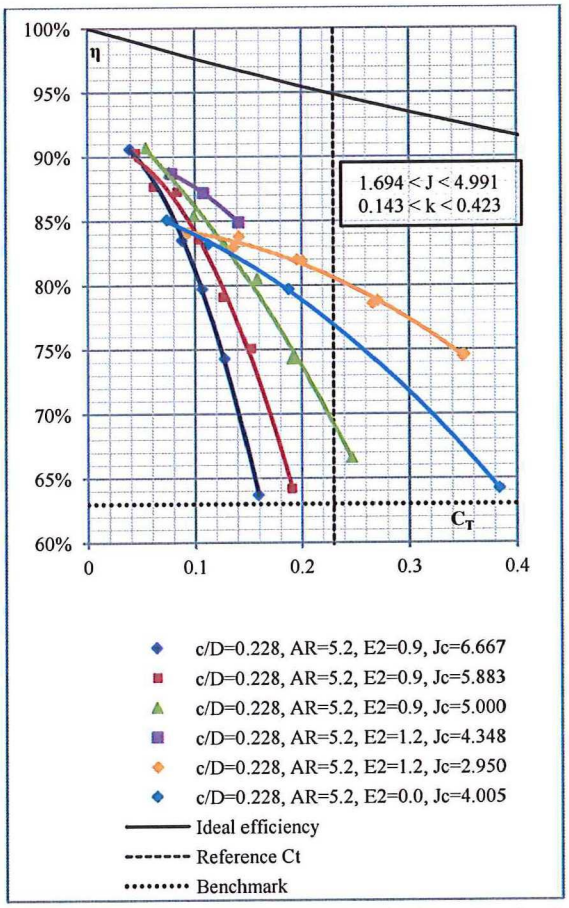

Figure 21. Effect of varying Critical-advance-ratio J_c on Efficiency versus C_T, for a single high *AR* fin held at constant chord-wise flexibility parameter E_2

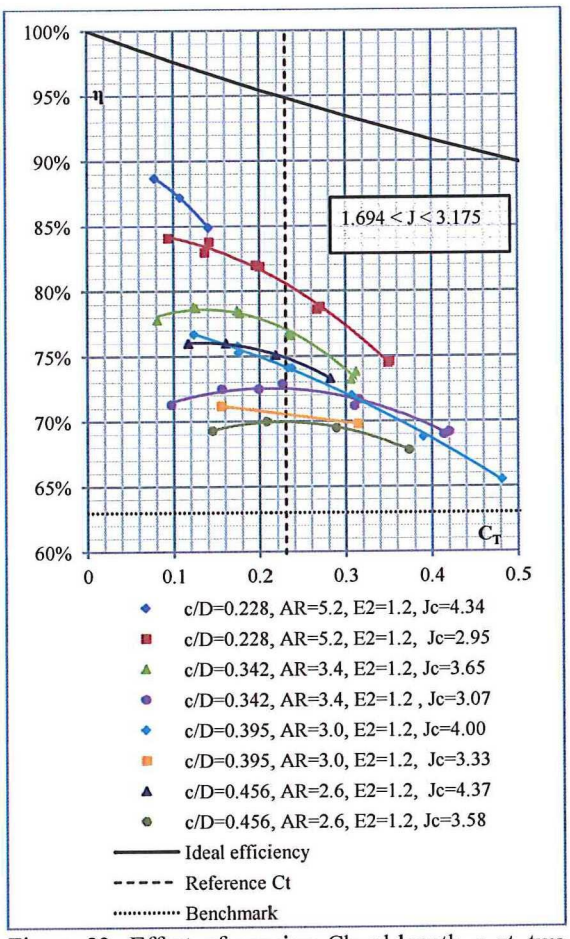

Figure 23. Effect of varying Chord-length *c* at two values of J_c on Efficiency versus C_T, for a single fin held at constant chord-wise flexibility parameter E_2

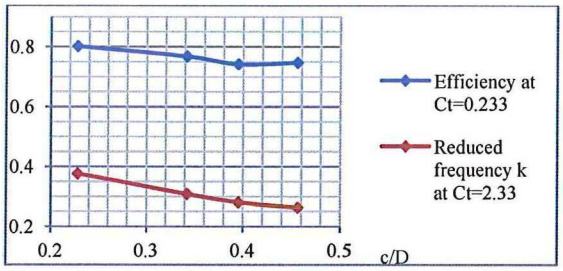

Figure 23. Interpolated values on best curve of figure 22 showing Efficiency and Reduced frequency as a function of chord length *c/D*

Effect of chord-length

Figure 22 confirms the previously determined trends: a decrease in J_c for the same fin causes the maximum efficiency to decrease while increasing the efficiency at a higher C_T.

Figure 22 also embodies an unexpected result of the measurement program: Fin efficiency is seen to diminish rapidly with increasing chord-length *c/D*, especially at low C_T. This decrease cannot be explained by a change in *AR* because the lift and span both do not vary, causing intensity of shed trailing edge vortices to remain constant at the same C_T. The decrease in efficiency can also not be explained by a total lift reduction and delay at unchanged viscous losses because the required lift is simply generated through a higher angle of attack: Figure 23 shows how efficiency decreases even as reduced frequency decreases. This sensitivity to chord-length reduces possibilities to avoid high transverse accelerations at markedly improved efficiency.

Performance of 2 fins on the same chariot

Increasing the number of fins on the chariot of the flapping propulsor has a much smaller effect on C_T than increasing the number of blades on a screw-propeller. The C_T increases slowly with decreasing ratio *Fin_gap / Stroke* as seen in figure 25, to reach a

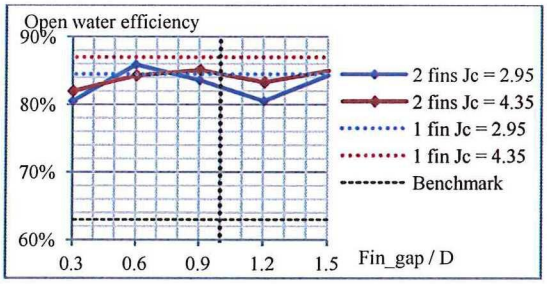

Figure 24. Effect on efficiency at same data as fig. 25.

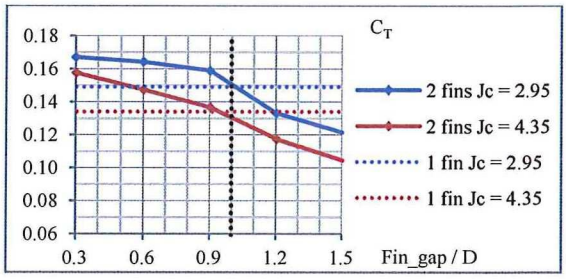

Figure 25. Effect of varying fin-distance of 2 flexible fins *AR* =5.2, *c/D* = 0.228, placed on the same chariot. {J_c =2.95, J=2.16, E_2=1.2} {J_c=4.35, J=2.85, E_2=0.9}

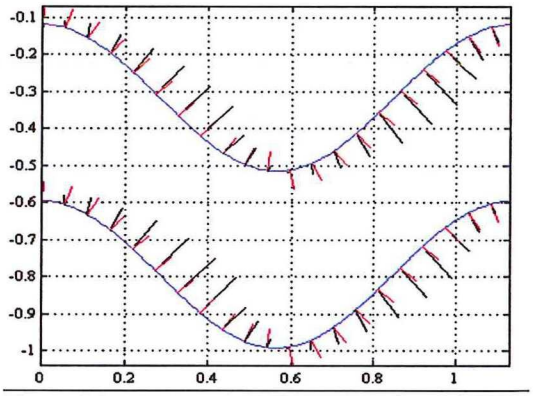

Figure 26. Visualisation of reaction force (black) on both fins at *fin_gap / D* = 1.2, J_c = 4.35. Fins moving to the right, distance in meters on X and Y axes. Red lines represent the normal direction to the path.

maximum value barely 20% above the single fin. This offers design flexibility in terms of stroke / ship width, but also puts an absolute ceiling to efficient C_T values.

Measurements with varying fin distance have been made with many changes of transducers; this increases the randomness of measurement inaccuracy. Also, the measurements at J_c = 2.95 were at the limit of the possibilities of the machine. High acceleration levels started to cause reduced stability of rotational speed: An FFT analysis shows 0.8% variation at the measurements done at J_c = 2.95 and 0.3% variation at the measurements done at J_c = 4.35. The effect of inaccuracy on C_T seems to be lower than that on efficiency. The accuracy of the general level in the efficiency graph is consistent with the rest of the program, but the validity of the pattern of variation with distance is less certain.

The general level of efficiency remains good when more than one fin is utilized. Figure 26 illustrates the generally observed pattern that the fin with the preceding suction-side has a higher reaction force (fins

moving to the right). We conclude that there is a marked decline in efficiency when the fin gap reaches 30% of stroke; this has been confirmed repeatedly. We dare conclude also that there is a possibility that a distance of 1.2 times the stroke is unfavorable at the tested value of chord-length to stroke. A practical conclusion from these measurements is that multi-fin operation cannot be expected to result in an increase of C_T higher than 10% without a loss in efficiency.

Performance when decreasing frequency stability

Variation of ω within the cycle, through a decrease of flywheel-inertia while keeping at constant drive torque, results in 0.6% loss of efficiency per % increase of fluctuation of drive-shaft speed in the range of measurable fluctuation with the machine. Three measurements were repeated twice at needed C_T with good repeatability, with a flexible fin with a relatively long chord. The range of fluctuation achievable with the experimental set-up was limited to 2.5% peak-to-peak. Within that range, the effect of fluctuation of angular shaft-speed on the performance of flapping propulsion is small, but conclusions the range of fluctuations cannot reliably be drawn.

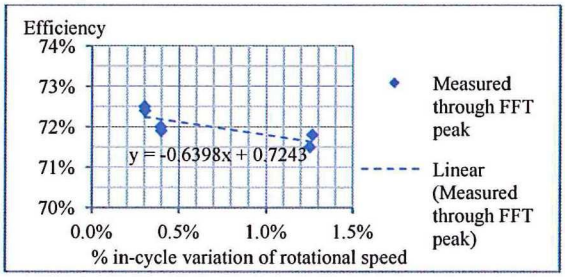

Figure 27. Effect of $\Delta\omega$ at C_T = 0.22, J = 2.56, J_c = 4.00, E_2 = 0.97, c/D = 0.39, AR = 3.0

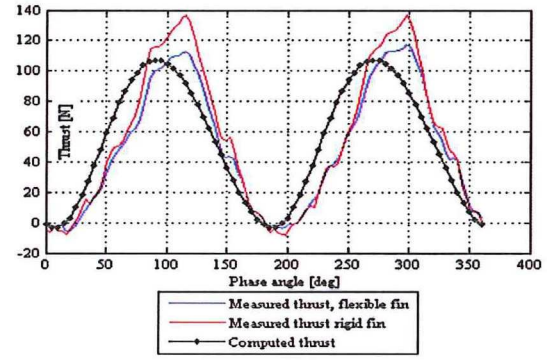

Figure 28. Instantaneous thrust as a function of phase angle of flexible fin, rigid fin, and predicted value by lifting-line approach

6. Results: details of one measurement

Table 10. Main parameters of the chosen measurement

Count of cycles	54	Speed V	1.978 m/s
Stroke D	0.396 m	Frequency N	1.815 Hz
Fin span	0.468 m	Average thrust T	49.8 N
Fin av. chord	0.090 m	σ(T)	0.4 N
Fin weight	1.12 kg	Thrust C_T	0.14
P_F (10% bending)	3670 Pa	OW efficiency	85.6%
J_c	4.35	Input power P_{tot}	120 W
Advance ratio J	2.75	Max pitching m^t	1.46 Nm
Reynolds	$1.95\ 10^5$	Rot. power P_{rot}	0.41 W
Red. frequency k	0.26	$C_{L\ max}$ (est.)	0.96
Flexibility E_2	1.23		

The presented measurement has parameters close to those needed in a re-engineered near-optimal machine that incorporates the results from this study. Data is shown as measured at scale 1/12. The measurement was part of a series where Critical advance ratio J_c and flexibility E_2 were kept constant, but where the load was varied through variation of speed and frequency. Froude scaling of the advance speed therefore does not result in 10.13 m/s. The measurement is of average quality. The thus obtained time-series are compared graphically to those obtained for the same operational parameters on a rigid fin, and to values projected by the analytical model developed in chapter 3. The measurements correspond to the two right-most points in Figure 19.

Figure 29 is representative of the stability of measurement seen in the program, where 54 cycles yield a narrow distribution. Absorbed power at first seems harmonic without phase-delay, which would challenge unsteady hydrodynamic theory. Inspection of the Figures 28 and 30 however, shows a phase-lag of the peak thrust and the peak reaction force of about 25 degrees compared to steady-state theory. Finally, Fig. 31, where the drag angle_becomes negative in the approach toward 180 degrees and 360 degrees, shows

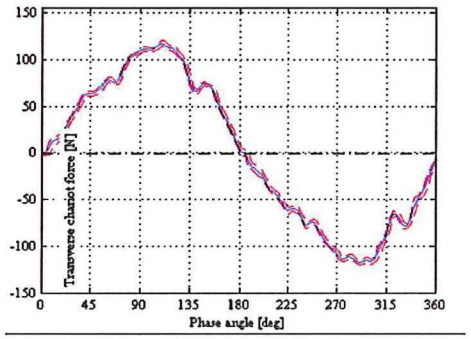

Figure 29. Projected transverse fin force and spread

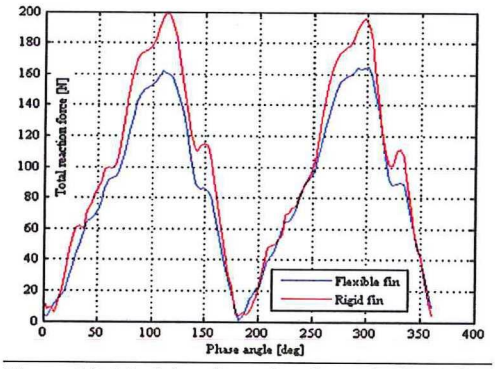

Figure 30. Module of reaction force for both fins

that the phase lag must also apply to lift direction. A missing variable is the mass acceleration force ($= M_{fin}D\omega^2/2$) that opposes the delayed reaction force at the ends of the stroke: 30 N in this case excluding added hydrodynamic mass. The mass acceleration force does not perform work, but does shift the phase of the heave forward to 0 degree phase angle, at least in this case. A near-triangular evolution of reaction force results, with a phase-synchronous base, and a 25 degrees phase-shift for the peak values as in Figure 30.

The utilized lifting-line estimator in chapter 3, also utilized in Figure 28 to forecast instantaneous thrust, was based on a 15 degrees phase lag as Figure 9 suggested, applied only to magnitude. Considering the fact that Reduced frequency k is only 0.26, we see from Fig. 28 that the analytical approach leads to underestimation of the phase delay and overestimation of lift reduction for this rigid fin. The estimator described in chapter 3 however provided a workable first order approach throughout the program. In this case the estimator predicts 54 N thrust where the rigid fin delivers 55.7 N, and the flexible fin delivers 49.8 N.

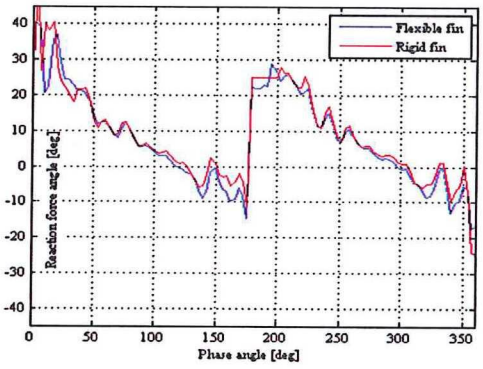

Figure 31. Computed drag angle of reaction force for flexible and rigid fin; clipped at ends of stroke

Comparing the pattern of the flexible fin and the rigid fin in Figure 30, we see that flexibility flattens the curve of the reaction force, but does not introduce any phase-shift. Figure 31 then shows that the saw-tooth pattern of drag angle is also very similar for the rigid and the flexible fin, except for the approach to 180 or 360 degrees of phase angle; the drag-angle of the rigid fin is then somewhat higher. This pattern explains the slightly better efficiency of the flexible fin: although the chord-shape has reverse camber at mid-stroke, there is no loss of efficiency, but there is a small gain of efficiency at the end of the stroke when making the turn. The observed saw-tooth pattern of the drag-angle suggests a pattern of energy storage and release with a discrete start at each stroke that would merit further investigation.

7. Conclusions and recommendations

Flapping propulsion for a container-feeder

A simple comparison of the energy losses of a screw-propeller and of a flapping propulsor showed that the gain from flapping propulsion originates from efficient blade operation even more than from a larger actuator surface. First order analytical estimation of thrust and efficiency predicted an open-water efficiency of 86% at design conditions for a container feeder with flapping propulsion. The benchmark-efficiency in this case is 63%, as measured with the design screw-propeller. 81% open-water efficiency was proven in the towing tank within the limits set by the purpose-built near-optimal flapping propulsor, by the range of available fin characteristics, and by time-constraints. This impressive 22% reduction in energy consumption would however be partially offset in practice by an anticipated lower hull efficiency and a lower mechanical efficiency. The magnitude of these losses is yet unknown, but could amount to a total of 10 - 15%.

For efficient flapping operation at the required loading conditions, we were seen to need fins with short chords, and a large pitching angle. To achieve the reference thrust coefficient C_T=0.23, we utilized a ratio *chord/stroke* of 0.23, an advance ratio $J = 2$ ($=V/DN$), and a critical advance ratio $J_c = 2.95$. The utilized fin was flexible chord-wise, but at this C_T, there appears to be no advantage. Froude scaling yields fins that operate at 107 m/s^2 transverse acceleration at a stroke $D = 4.75$ m. Attempts to reduce acceleration (increase J) through fitting fins with longer chords proved to decrease efficiency. Multi-fin operation proved a poor option to decrease fin-loading as well. Acceleration forces for the flapping machine at a high efficiency of

operation can only be reduced through a combination of increased stroke, rigid fins, and a reduction of required thrust loading C_T through increased actuator width. This latter route also shows material promise for further improvement: a C_T of 0.11 would mean a further 5% gain in open-water efficiency. The best measurement so far – within the constraints defined by the ship and the machine – still falls short of translating into a break-through propulsor when implementation losses are taken into account. Further research concerning the flapping machine should therefore be directed at increasing the effective actuator width, and further research on fins should be aimed at generating more data in the neighborhood of the identified efficient area of parameters where *chord/stroke* = 0.23.

General conclusions for flapping propulsion

Three clear results emerged from the program:

- A first map of achievable efficiency of flapping marine propulsion for the range of thrust coefficients $0.05 < C_T < 0.35$ is now available, with an indication of the required chord-length and the critical advance ratio J_c
- The efficiency of flapping propulsion decreases with increasing chord-length to stroke ratio without direct relation to a decreasing AR or an increasing reduced frequency
- Increasing pitching angle decreases slowly the best achievable efficiency, but increases efficiency at higher loading substantially; there is no rapid drop in efficiency due to decreasing advance ratio J if the critical advance ratio J_c decreases too.

Unsteady analytic theory as proposed by Theodorsen (1935) provided a workable first-order approach for thrust prediction. This approach however cannot provide a prediction of relative efficiency performance when chord-length & pitching amplitude are both varied. Further investigation on this subject is recommended.

Prempaneerach, *et al.* (2003), measured efficient flapping propulsion with chord-wise flexible foils at $\mathrm{Re} = 4.10^4$ and chord to stroke ratio $c/D = 0.66$, and measured common best values at 70% efficiency approximately. For the highest ratio chord-length to stroke that we tested at $c/D = 0.46$ and $R_e = 2.10^5$ in turbulent flow, we found similar values at model scale with a flexible fin. At (efficient) short chord $c/D = 0.23$, low thrust loading $C_T < 0.2$ and $R_e = 2.10^5$ we found a weak positive efficiency effect from chord-wise flexibility only We found the positive effect of chord-wise flexibility to vanish with decreasing pitching amplitude and with increasing C_T. E_2, the dimensionless measure of chord-wise flexibility that we chose, provided a good forecast of flexibility-induced thrust-reduction in the cases where we could compare directly, but needs experimental validation over a broader range of chord-lengths and rotation amplitudes to become a robust predictor. E_2 did prove not to be a valuable predictor of the magnitude of the efficiency effect of chord-wise flexibility. We are unaware of any non-dimensional characterization of chord-wise flexibility that works well with respect to predicting efficiency gain. This would merit further investigation to reduce the number of tests needed at varying chord-length and varying pitching amplitude■

References

Abbot, I., Von Doenhoff, A., 1949, "Theory of wing sections", Appendix IV, NACA 63015 profile

Anderson, J. M., Streitlien, K., Barrett, D.S., Triantafyllou, M.S., "Oscillating foils of high propulsive efficiency" Journal of fluid mechanics, Vol. 360, 1998, pp.41-72

Fish, F.E., Rohr, J.J., 1999, "Review of Dolphin Hydrodynamics and Swimming performance", SSC San Diego Technical report 1801

Hover, F.S., Haugsdal, Ø, Triantafyllou, M.S., Effect of angle of attack profiles in flapping foil propulsion" Journal of fluids and structures, Vol. 19, 2004, pp. 37-47

Katz, J., Weihs, D., "Hydrodynamic propulsion by amplitude oscillation of an airfoil with chordwise flexibility" Journal of Fluid Mechanics, Vol. 88, part 3, 1978, pp. 485-497

Prempraneerach, P., Hover, F.S., Triantafyllou, M.S., "The effect of chordwise flexibility on the thrust and efficiency of a flapping foil", 13th Intern. Symp. Unmanned Untethered Submersible Techn., Durham, NH., Aug. 24-27, 2003.

Sherer, O., "Experimental and theoretical investigation of large amplitude oscilating foil propulsion systems", May 1968, Hydronautics Incorporated, Washington DC

Shouveiler, A. Hover, F.S., Triantafyllou, M.S. "Performance of flapping foil propulsion" Journal of fluids and structures, Vol. 20, 2005, pp. 949-959

Theodorsen, T., 1935. "General theory of aerodynamic instability and the mechanism of flutter". NACA report 496

Acknowledgement

The authors are much indebted to A.P. Moller Maersk A/S for its longer term R&D policy and its commitment to sustainable technology development that made this study possible.

DISCUSSION

Michael Triantafyllou
Massachusetts Institute of Technology, USA

This is a comprehensive paper, exploring the use of flapping foils for ship propulsion. Model tests at 1-to 12-scale provide valuable confirmation of the theoretical predictions. The intriguing differences between conventional ship propulsion and fish-like propulsion is a continuous source of inspiration for studies using foils, flexible foils, or even flexible bodies to propel marine craft; yet, to date, only experimental and exploratory vehicles have been designed and constructed.

This study first addresses what is the main benefit to be had from using this new technology. The answer is simple in principle, viz. that there is potential for a larger swept area compared to propellers, while other hydrodynamic effects (well outlined in the paper) contribute to high efficiency; but there are many complex details to consider as well.

The flipside, i.e. the disadvantages, are obvious, as for any new technology that has to compete with an existing technology that is over a century old: principally, that conventional driving mechanisms are not well-suited to oscillatory propulsion. With the advent of artificial muscles this may be remedied, but for the time being such actuators are neither efficient nor reliable for long-term, continuous use.

In the paper by Varmeiden et al, a conventional engine is envisioned, modified to actuate the harmonic driving of the flapping fins, which by necessity involves large inertia loads. In model scale such systems work well. In 1995, Triantafyllou & Barrett provided a design for a conventional actuation mechanism driving mechanism. In 1996, Czarnowski built and tested a 12 ft model that demonstrated that the ship model could be driven effectively by such flapping foils.

The paper is clearly of high quality and the authors are to be congratulated for such a comprehensive, experiment-supported study. In the interest of further clarifying the issues addressed in the paper, and in the hope that the study will lead to a commercial application soon, I offer the following analysis and provide the following comments and questions (I provide only those references that are not quoted in the paper):

The study in Anderson et al 1998 for a foil with given geometry (aspect ratio and profile), and given amplitude to chord ratio, identified two major parameters affecting performance: (a) the Strouhal number St (which is the inverse of J as used in this paper), which is optimal, due to wake considerations, in the range of 0.2 to 0.4 (expressed in J, optimality requires J to be in the range of 2.5 to 5); and (b) the maximum angle of attack, which should be around 20 to 30 degrees. Hover et al (2003) added a third parameter, the content of high harmonics in the angle of attack – the less the better; i.e. a purely sinusoidal angle of attack produced a "pure" reverse Karman street that was found to have clearly the best efficiency. Throughout these studies, it was found that higher amplitude to chord ratios improved efficiency. The study of Prempraneerach et al (2005) showed a beneficial impact on efficiency from properly selected foil flexibility; from the flow visualizations of Hover et al (2003) it appears that, again, the reason is that under
optimal flexibility conditions there results the formation of a pure reverse Karman street
– unlike the formation of multiple-vortex per cycle patterns under non-optimal conditions. Hence flexing is favorable when it prevents the formation of multiple vortices per cycle.

The following questions arise:
-- First, as mentioned by the authors, the added mass terms do not add or subtract energy. This, however, presumes that somehow the system can take back energy, when appropriate, and then return it when needed. The use of lateral springs to mount the foils would provide a setting where, under near-resonance conditions, this can be accomplished. It is a well-known fact that animals use this mechanism to minimize expended energy. How would this affect the design of the system?
-- The most likely reason for the effect of flexibility is to produce a single Karman street.
Flow visualization will confirm this hypothesis and also set a better way to define the proper optimal flexibility or stiffness.
-- The sensitivity of chord to length may simply be due to the sensitivity of the efficiency to the ratio of the amplitude of motion to chord length.
-- The paper addresses extensively the impact of heave and pitch motions; however, it is better to use the angle of attack instead of the pitch angle. Both the amplitude and high harmonic content of the angle of attack versus time play a significant role in thrust development and energy expenditure.

AUTHORS' REPLY

The authors thank Mr. Triantafyllou for his involvement and his remarks.

Mr. Triantafyllou cites a number of papers with experimental results among which the study of Anderson et al (1998) where the most efficient advance ratios J (= 1/Strouhal) are to be found between 2.5 and 5 and where the maximum angle of attack should be around 20 to 30 degrees.

We found that the most efficient advance ratios J are not necessarily limited to that range. We found that they can be lower, and that they are dependent on both:

- The ratio Chord-length / Amplitude
- The rotation amplitude of the fins

We also found very clearly and systematically that the most efficient estimated maximum angle of attack is 10 to 11 degrees in the range of parameters where we performed the measurements, and not 20 to 30 degrees.

It is to be noted that in the parameter range where we performed the measurements, we could not reproduce a large gain in efficiency due to chord-flexibility as described by Prempaneerach et al. (2005). The higher Reynolds number utilized in our experiments could possibly provide part of the explanation due to delayed separation in turbulent flow.

Adding lateral springs to the system. The mechanical system is additive, so lateral springs could be fitted in principle as a variation on the flywheel approach that we chose. Adding springs would result in:

- More difficult operation away from the resonance frequency, and would make the system harder to start
- Operation of the system with more harmonics which would cause break-down of the near-optimum cycle of angle of attack of the single-shaft mechanism

Sensitivity to chord length. Although some of the mentioned publications do mention a positive effect of shorter chord-lengths, no paper has given this phenomenon the attention it deserves in our view, either in terms of magnitude of impact or in terms of tested parametric range. We found low chord-length to amplitude to be the key parameter to achieve high efficiency flapping propulsion, much more than small variations of angle of attack or advance ratio. We also found that the effect is much larger than can be explained by aspect ratio or reduced frequency.

Using angle of attack instead of using the pitch angle. In our view both the angle of attack and the pitching angle are important in a totally different manner:

- The angle of attack can be estimated but cannot be measured due to the unknown local velocity of the induced flow. We utilize angle of attack for design of the experiments, but not for measurement. No towing tank reports angle of attack for propulsion measurements because it cannot be measured but can only be inferred. We therefore define a measurement in terms of the advance ratio and the critical advance ratio at which it happened.
- The pitching angle of the fins can be compared to the propeller pitch. Changing the pitching angle changes the propulsive behavior completely and translates in different parameters for highest thrust, highest efficiency and needed input torque at given speed.

DISCUSSION

Qiang Zhu
University of California San Diego, USA

This paper reports an experimental investigation of a novel propeller including multiple flapping foils. Each foil undergoes periodic heaving and rotational motions imitating aquatic animals. Mechanically, the innovation lies in a single device to generate the heaving and rotating motions simultaneously. Although these motions are not sinusoidal, the time history of the variation of the effective angle of attack is smooth without the wobbles in similar experimental devices that are believed to deteriorate the thrust generation performance. Theoretical predictions based on the lifting line theory are also conducted. The unsteady effects are approximated using Theodorsen's theory. Although a major shortcoming of this approach is the total negligence of the leading edge vortices, in the cases considered in this study the effective angle of attack is sufficiently small so that the effect of LEV is not significant.

One of the focuses of this study is on the effects of structural flexibility upon the propulsion performance. Through a few tests the conclusion is that the performance enhancement is not significant. However, we know that the fluid-structure interaction involved in the dynamics of flexible foils is a complicated problem. The overall effect of deformability depends on issues such as the structural stiffness as well as the kinematics of foil motion. Specifically, it was found that certain amount of

flexibility reduces the dependence on kinematic parameters. Its beneficial effect is most pronounced in combinations of kinematic parameters that are less favorable for thrust generation. For example, the authors may try a case in which the foil motion is purely in the heaving mode. In that case the difference between a rigid foil and a flexible one should be larger.

Another focusing point of this study is the use of multiple foils. One of the advantages of using multiple foils is that the lateral forces generated by these foils can be cancelled to avoid zigzagging. In addition, it may be interesting to study the effect of different phases between the foils. This is not discussed in this paper. In fact, herein the foils have the same phase, producing a stronger lateral force.

AUTHORS' REPLY

The authors thank Mr. Zhu for his involvement and his remarks.

The objective of the investigations presented in this paper is to provide input for fact based evaluation on how economically relevant flapping propulsion could become for merchant shipping. This required us to be focused on identifying parameter areas where propulsion is highly efficient given geometry constraints typical of a merchant vessel.

Effect of chord-wise flexibility. We have had to do our best to avoid loosing time with measurements too far outside the highest propulsive efficiency area. We therefore have no analysis of the effect of chord-wise flexibility when the parameters are not near-optimal. Within the range of parameters where flapping propulsion is materially more efficient than propellers, we did manage to put together a good set of measurements where performance with flexible fins could be compared to performance with rigid fins. These are not just a few measurements as could be understood in Mr. Zhu's remarks, but more than 35 full runs with angles of attack varying between 4 and 20 degrees and with rotation amplitude varying between 25 and 38 degrees.

Multi-fin operation. We agree with Mr. Zhu's remarks. The reason for the chosen set-up is that the lateral forces are compensated internally by a translating internal chariot to avoid a second seal. A system with two opposed chariots could indeed be studied. Phase variation between the two chariots is especially relevant to study vortex interaction when one fin operates downstream of the other. In fact the utilized machine is equipped with a facility to do exactly that, but this study has not yet been conducted.

Theodorssen and leading edge vortices. We found prediction utilizing analytical theory broadly workable in the range until 20 degrees of angle of attack. The high Reynolds number (200.000) chosen for the conducted experiments could possibly play a role in delaying leading edge separation compared to what happens in the range of Reynolds numbers typically utilized for unmanned submersibles or for biological analysis.